

Isotopic composition of convective rainfall in the inland tropics of Brazil

Vinicius dos Santos¹, Didier Gastmans¹, Ana María Durán-Quesada², Ricardo Sánchez-Murillo³, Kazimierz Rozanski⁴, Oliver Kracht⁵ and Demilson de Assis Quintão⁶.

¹São Paulo State University (UNESP), Environmental Studies Center. Av. 24ABased, 1515, Bela Vista, 13.506-900, Rio Claro, São Paulo, Brazil. vinicius.santos16@unesp.br; didier.gastmans@unesp.br

²Escuela de Física & Centro de Investigación en Contaminación Ambiental & Centro de Investigaciones Geofísicas, Universidad de Costa Rica, San José 11501, Costa Rica. ana.duranquesada@ucr.ac.cr

³University of Texas at Arlington, Department of Earth and Environmental Sciences, 500 Yates Street, Arlington, Texas 76019, USA. ricardo.sanchezmurillo@uta.edu

⁴Faculty of Physics and Applied Computer Science, AGH University of Krakow, al. Mickiewicza 30, 30-059 Krakow, Poland. Faculty of Physics and Applied Computer Science, AGH University of Science and Technology, al. Mickiewicza 30, 30-059 Krakow, Poland. rozanski@agh.edu.pl

⁵International Atomic Energy Agency, Isotope Hydrology Section, Vienna International Centre, P. O. Box 100, 1400 Vienna, Austria. O.Kracht@iaea.org

⁶São Paulo State University (UNESP), IPMet/Science College, Est. Mun. José Sandrin IPMET, S/N, 17.048-699, Bauru, São Paulo, Brazil. demilson.quintao@unesp.br

Correspondence to: Didier Gastmans (didier.gastmans@unesp.br)

Abstract. ~~The tropical central southern part of Brazil (CSB) is characterized by strong convective systems bringing generous water supply for agro-industrial activities but also pose flood risks for large cities. Here, we present high-frequency (2–10 minutes) rainfall isotopic compositions to better understand those systems, with a total of 90 intra-event samples collected during the period 2019–2021. Combining intra-event and inter-event analysis it is explained how regional and local meteorological processes control the isotope variability within 8 convective rainfall events. While convective activity, associated with outgoing longwave radiation (OLR) and moisture transport, evaluated from Hysplit modelling and ERA-5 eastward vapor flux, modulate the seasonal rainwater isotopic composition. Low $\delta^{18}\text{O}$ values (median $< -6.8\%$) were observed during summer, when lower OLR and predominantly moisture influence from Amazon Forest), while high values (median $> -4.2\%$) during autumn and spring, when higher OLR and moisture from Atlantic Ocean and South Brazil are acting. A semi-quantitative evaporation model evaluated local influences in summer convective events, revealing distinct isotope characteristics between day (high $\delta^{18}\text{O}$, low d excess and substantial evaporation) and night (low $\delta^{18}\text{O}$, high d excess and negligible evaporation). Our results offer a new framework of key drivers controlling the isotopic variability of rainfall in tropical South America that must be considered in future studies of convective systems across the tropics. The tropical central-~~

Código de campo alterado

Código de campo alterado

southern region of Brazil is characterized by strong convective systems. These systems provide abundant water for agro-industrial activities but also pose flood risks to large cities. Here, we present high-frequency (2-10 min) rainfall isotopic compositions (n=90 samples) to reveal the regional and local atmospheric processes controlling the isotopic variability of convective systems from 2019-2021. Isotope parameters from individual events, including initial (δ_{initial}), median (δ_{med}), and the difference between lowest and highest isotope values ($\Delta\delta$), and detailed meteorological data, were used in inter-event and intra-event analysis. The lower δ_{initial} values were associated with higher rainfall along Hysplit trajectories from the Amazon forest during the summer, compared to autumn and spring, when Hysplit trajectories from the Atlantic Ocean and South Brazil had lower amounts of rainfall. Consequently, there were high δ_{initial} values. This regional δ -signature was conserved during certain convective intra-events, with similar values between the δ_{initial} and δ_{median} . However, for other intra-events, the δ_{initial} values were altered by local processes connected to cloud features, rainfall vertical structure, and humidity conditions, resulting in increased isotopic variations ($\Delta\delta$) during intra-events. Our findings establish a novel framework for evaluating the meteorological controls on the isotopic variability of convective precipitation in tropical South America, fill the gap of high-frequency studies in this region, and generate a comprehensive meteorological dataset for future modeling studies.

Formatado: Inglés (Reino Unido)

1 Introduction

The central-southern part of Brazil (CSB) is the main contributor to the Brazilian economy, with agriculture and industry as leading activities (Zilli et al., 2017). These sectors strongly depend on rainfall seasonality for irrigation and hydropower supply (Luiz Silva et al., 2019). Suggested changes in frequency of heavy and extreme rainfall events in future climate scenarios (Marengo et al., 2020; Donat et al., 2013; IPCC, 2021) may represent a serious threat to regional economic activities and electricity generation. Similarly, climate projections also suggest that enhancement of heavy rainfall events will aggravate the occurrence of both floods and landslides across vulnerable areas (Marengo et al., 2020), whose total cost has risen to US\$ 41.7 billion in the past 50 years (Marengo et al., 2020; World Meteorological Organization, 2021). The tropical central-southern region of Brazil (CSB) is the primary contributor to the country's economy, with agriculture and agroindustry as the main sectors (Zilli et al., 2017). These economic activities are highly dependent on seasonal rainfall for irrigation and hydropower supply (Luiz Silva et al., 2019). Projected changes in the frequency of heavy and extreme rainfall events in future climate scenarios (Marengo et al., 2020; Donat et al., 2013; IPCC, 2021; Marengo et al., 2021) pose a significant threat to regional economic enterprises and power generation. Similarly, according to Marengo et al. (2021), simulations with the pre-CMIP6 models suggest that the intensification of heavy rainfall events could exacerbate the prevalence of floods and landslides in susceptible regions. Such occurrences have resulted in a total cost of US\$41.7 billion over the past half-century (Marengo et al., 2020; World Meteorological Organization, 2021).

65 Extreme rainfall events are related-linked to the convective systems (CS), characterized by strong vertical development in
the form of cumulus-nimbus and cumulus congestus (convective clouds) and low-level divergence (stratiform clouds) (Siqueira
et al., 2005; Machado and Rossow, 1993; Zilli et al., 2017; Houze, 1989, 2004), commonly refer to as convective and stratiform
rainfall, that account for 45% and 46% of the total rainfall in South America, respectively (Romatschke and Houze, 2013).
70 These rainfall types have recently been postulated as a major driver explaining variations in stable isotope composition of
precipitation across the tropics (Zwart et al., 2018; Sánchez-Murillo et al., 2019; Sun et al., 2019; Han et al., 2021; Aggarwal
et al., 2016). Specifically, the role of tropical convection in formation of the isotopic composition of rainfall has been discussed
in the context of so-called amount effect (heavy isotope contents of tropical precipitation decrease as the amount of local
precipitation increases) (Dansgaard, 1964; Hu et al., 2018; Kurita, 2013; Rozanski et al., 1993; Winnick et al., 2014;
Tharammal, T., G. Bala, 2017). The CS significantly contribute proportion of annual rainfall and account for a significant
75 portion of extreme rainfall (Roca and Fiolleau, 2020). Across the tropics, diurnal surface heating amplifies convection,
generating short-lived events that can occur in consecutive days. Rapid upward movement of air results in quick condensation
and formation of precipitation with substantial droplets and heavy rainfall (Breugem et al., 2020; Kastman et al., 2017; Lima
et al., 2010; Machado et al., 1998). This is identified by vigorous vertical development in the form of cumulus-nimbus and
cumulus congestus (convective clouds) and low-level divergence (stratiform clouds) (Siqueira et al., 2005; Machado and
80 Rossow, 1993; Zilli et al., 2017; Houze, 1989, 2004). Precipitation associated with these systems are commonly referred as
convective and stratiform rainfall, and account for 45% and 46% of the total rainfall in South America, respectively
(Romatschke and Houze, 2013).

Previous studies used satellite retrievals of atmospheric water vapor isotopic composition to better understand convective
processes in other regions (Lawrence et al., 2004; Worden et al., 2007; Kurita, 2013). They showed the links between the
85 structure and depth of convective systems as well as variations in the isotopic composition of local vapor (e.g. Lekshmy et al.,
2014; Vuille et al., 2003; dos Santos et al., 2022). Despite these advances, to date only few studies have examined the rainfall
isotopic composition in the light of diurnal variations in convective activity of tropical atmosphere (Munksgaard et al., 2020;
Moerman et al., 2013).

Diurnal variations in heating of the surface intensify convection processes, generating short-lived events that can occur in
90 consecutive days across the tropics (Romatschke and Houze, 2013, 2010). These events are characterized by a diurnal cycle
and notable differences in: (i) rainfall intensity, (ii) vertical extent of convective cores between deep and shallow convection,
and (iii) life cycle of these events in mesoscale convective systems (MCSs) (Schumacher and Houze, 2003; Romatschke and
Houze, 2013, 2010). Convective events account for a significant proportion of annual rainfall and are linked with extreme
events over the land, with most intense events occurring in the afternoon (Schumacher and Houze, 2003; Kurita, 2013; Wang
95 and Tang, 2020). High-frequency rainfall sampling strategies during the occurrence of convective events are needed to capture
the diurnal heating cycle and associated variations in the isotopic signatures of convective rainfall.

Código de campo alterado

Whether rainfall is convective or stratiform rainfall has been suggested to determine variations in stable isotope composition of precipitation across the tropics (Zwart et al., 2018; Sánchez-Murillo et al., 2019; Sun et al., 2019; Han et al., 2021; Aggarwal et al., 2016; Munksgaard et al., 2019).

100 Processes driving the variations in the isotopic composition in convective systems are more complex and less understood compared to the case of other precipitation producing systems (de Vries et al., 2022). Studies using the isotopic composition of rain and water vapor have quantified and modelled physical processes related to convection (Bony et al., 2008; Kurita, 2013). Previous studies have suggested that the isotopic composition of convective systems is connected to the integrated history of convective activity (Risi et al., 2008; Moerman et al., 2013), depth of organized convection and aggregation
105 (Lawrence et al., 2004; Lekshmy et al., 2014; Lacour et al., 2018; Galewsky et al., 2023), microphysical processes within clouds (Aggarwal et al., 2016; Lawrence et al., 2004; Zwart et al., 2018), and cold pool dynamics (Torri, 2021). These interpretations simplified and lumped the effects of multiple rainfall timescales (e.g. monthly, daily and high frequency), providing different perspectives on convective processes, such as the regional (synoptic forcings) and local factors (e. g. microphysical processes occurring both within and below the cloud) (Kurita et al., 2009; Muller et al., 2015).

110 High-frequency rainfall sampling and analyses of stable isotope ratios has been used to better understand the evolution of large weather systems such as tropical cyclones and typhoons (Sun et al., 2022; Sánchez-Murillo et al., 2019; Han et al., 2021), squall lines (Taupin et al., 1997; Risi et al., 2010; Tremoy et al., 2014) and local evaporation effects (Graf et al., 2019; Aemisegger et al., 2015; Lee and Fung, 2008). ~~This high-resolution isotope information provided a better insight into the development of weather systems and cloud dynamics, both responsible for changes in the rain type, intensity, and inherent isotope variability during rainfall events (Coplen et al., 2008; Muller et al., 2015; Celle-Jeanton et al., 2004). Nevertheless, high frequency isotope sampling of rainfall has been limited across the tropics, despite convective activity being significant in this region.~~

120 ~~Using high-frequency rainfall sampling strategy we focus here on processes controlling isotopic composition of convective rainfall, which are of local (below cloud evaporation and isotope exchange processes, vertical structure of rainfall, cloud top over sampling site, and others) and regional (moisture origin/transport, regional atmospheric circulation). We combine high-frequency rainfall sampling with ground-based observational data (Micro Rain Radar, and automatic weather station) with satellite imagery (GOES-16), ERA-5 reanalysis products and HYSPLIT trajectories to characterize convective rainfall collected over the inland tropics of Brazil.~~

125 In this study, we used high-frequency rainfall sampling to investigate regional (moisture origin/transport, regional atmospheric circulation) and local (below-cloud processes, vertical structure of rainfall, cloud top temperature) processes that controlling the isotopic composition of convective rainfall. High-frequency rainfall was integrated with ground-based observational data (Micro Rain Radar and automatic weather station), satellite imagery (GOES-16), ERA-5 reanalysis products, and HYSPLIT trajectories to better characterize convective rainfall over the inland tropics of Brazil.

2 Data and Methods

2.1 Sampling site and weather systems

The rainfall sampling site was localized in Rio Claro city, São Paulo State (Fig. 1a). The station (-22.39°S, -47.54°W, 670 m.a.s.l.) ~~belongs to is part of the~~ Global Network of Isotopes in Precipitation network (GNIP) and is influenced by weather systems responsible for rainfall variations and seasonality linked to the regional atmospheric circulations of CSB region. The rainfall seasonality over CSB is associated with: (i) frontal systems (FS), represented mainly by cold fronts from southern South America acting all the year, and (ii) the South Atlantic Convergence Zone (SACZ) during austral summer (December to March) (Kodama, 1992; Garreaud, 2000) (Fig. 1b). These synoptic features are mostly responsible for the development of CS (Romatschke and Houze, 2013; Siqueira et al., 2005; Machado and Rossow, 1993) (Fig. 1c), and were captured during their passage over the Rio Claro station.

2.2 Rainfall sampling and isotope analyses

High-frequency sampling of rainfall events was done manually with the aid of passive collector (ca. 2 to 10 minutes intervals) from September 2019 to February 2021, except for April, July, and August (during winter 2020), when no rainfall was observed in the study area. ~~Due to the difficulties of manual sampling and uncertainties involved in forecast of rainfall occurrences for one point, rainfall events were collected randomly during the monitoring period. Covid-19 restricted access at the university, which resulted in fewer rainfall events sampled, mainly at night during spring 2020. The rainfall samples collected in this study generally do not represent consecutive pairs of day-night data during the same day. Daytime data are related to rainfall samples collected at Rio Claro station from 07:00 to 18:59 local time (10:00-21:59 UTC) whereas night time data represent the period 19:00-06:59 local time (22:00-09:59 UTC). In total, 90 samples representing eight convective events (3 night-time events and 5 day-time events) have been collected. The collected samples were transferred to the laboratory and stored in 20 mL HDPE bottles at reduced temperature (+4°C). In parallel to high-frequency sampling, monthly cumulative rainfall samples were also collected at the Rio Claro site during the study period as a contribution to the GNIP network, using the methodology recommended by the International Atomic Energy Agency (IAEA, 2014). Covid-19 disrupted access to the university, thereby reducing the number of rainfall events sampled during the spring of 2020, particularly at night (e.g., lockdowns). In this study, the rainfall samples collected do not consist of consecutive day-night pairs during the same day. In total, 90 samples representing eight convective events (3 night-time and 5 day-time events) were collected. Samples were transferred to the laboratory and stored in 20 mL HDPE bottles at 4 °C. In parallel to high-frequency sampling, monthly cumulative rainfall samples were also collected at the Rio Claro site during the study period as a contribution to the GNIP network, using the methodology recommended by the International Atomic Energy Agency (IAEA, 2014).~~

2.3 Isotope analyses

Rainfall samples were analysed for stable isotope composition using Off-Axis Integrated Cavity Output Spectroscopy (Los Gatos Research Inc.) at the Hydrogeology and Hydrochemistry laboratory of UNESP's Department of Applied Geology and at the Chemistry School of the National University (Heredia, Costa Rica). All results are expressed in per mil relative to Vienna Standard Mean Ocean Water (V-SMOW). The certified calibration standards used in UNESP were USGS-45 ($\delta^2\text{H} = -10.3\text{‰}$, $\delta^{18}\text{O} = -2.24\text{‰}$), USGS-46 ($\delta^2\text{H} = -236.0\text{‰}$, $\delta^{18}\text{O} = -29.80\text{‰}$), including one internal standard (Cachoeira de Emas - CE - $\delta^2\text{H} = -36.1\text{‰}$, $\delta^{18}\text{O} = -5.36\text{‰}$). USGS standards were used to calibrate the results on the V-SMOW2-SLAP2 scale, whereas CE was used for memory and drift corrections. In Costa Rica laboratory, the certified standards MTW ($\delta^2\text{H} = -130.3\text{‰}$, $\delta^{18}\text{O} = -16.7\text{‰}$), USGS45 ($\delta^2\text{H} = -10.3\text{‰}$, $\delta^{18}\text{O} = -2.2\text{‰}$), and CAS ($\delta^2\text{H} = -64.3\text{‰}$, $\delta^{18}\text{O} = -8.3\text{‰}$) were used to correct the measurement results for memory and drift effects and to calibrate them on the V-SMOW2-SLAP2 scale (García-Santos et al., 2022). The analytical uncertainty (1σ) was 1.2‰ for $\delta^2\text{H}$ and 0.2‰ for $\delta^{18}\text{O}$ for UNESP analysis and 0.38‰ for $\delta^2\text{H}$ and 0.07‰ for $\delta^{18}\text{O}$ for Costa Rica analysis. Deuterium excess (*d*-excess) was calculated as: $d\text{-excess} = \delta^2\text{H} - 8 \cdot \delta^{18}\text{O}$ (Dansgaard, 1964). Its uncertainty $1(\sigma)$ resulting from the uncertainties of the isotope analyses was equal 1.33 and 0.43‰, respectively. This secondary isotope parameter was used to interpret the influence of moisture origin/transport (Sánchez-Murillo et al., 2017; Froehlich et al., 2002) and to quantify below-cloud processes (e.g. Jeelani et al., 2018; Graf et al., 2019; Aemisegger et al., 2015).

2.4 Meteorological data

Automatic Weather Station (AWS) Decagon Em50 (METER) was installed near the Micro Rain Radar (MRR) (METEK) at 670 m.a.s.l, in immediate vicinity of the rainfall collection site. Meteorological data were recorded at 1 min intervals for rain rate (AWS RR, $\text{mm}\cdot\text{min}^{-1}$), air temperature (T, °C) and relative humidity (RH, %). The MRR data for reflectivity (Z, dBZ), and fall velocity (*w*, $\text{m}\cdot\text{s}^{-1}$) were also recorded at 1 min intervals. MRR parameters correspond to the mean values measured at the elevation between 150 and 350 meters above the local ground. MRR operated at a frequency of 24.230 GHz, modulation of 0.5 – 15 MHz according to the height resolution mode. For this work, different height resolutions (31 range bin) were tested, 150m, 200m, 300m and 350m, resulting in vertical profiles of 4650m, 6200m, 9300m and 10.850m, respectively (Endries et al., 2018). The MRR data used in the following discussion are the near-surface data (first measurement from 150m to 350m). The MRR data used in the following discussion are the near-surface data (first measurement from 150 m to 350 m). The MRR vertical profile (from 150m to 10,850m) was used to classify and visualize the radar echoes. Lifting Condensation Level (LCL, meters) was computed from AWS RH and T, using expression proposed by Soderberg et al. (2013).

GOES-16 imagery (https://home.chpc.utah.edu/~u0553130/Brian_Blalock/cgi-bin/goes16_download.cgi) was used to identify the convective nuclei of the cloud-top (10.35- μm , Band-13) and brightness temperature (BT), at 10 min intervals during the sampling period (Ribeiro et al., 2019; Schmit et al., 2017). The 10.35- μm BT is often used to estimate the convective

cloud depth, since the lower BT is linked to deeper cloud tops (Adler and Fenn, 1979; Roberts and Rutledge, 2003; Adler and Mack, 1986; Ribeiro et al., 2019; Machado et al., 1998).

195 The weather systems (Frontal, instabilities and low pressure) were defined according to the synoptic chart (<https://www.marinha.mil.br/ehm/dados-do-smm-cartas-sinoticas/cartas-sinoticas>) and meteorological technical bulletin of the Center for Weather Forecast and Climatic Studies of the National Institute of Space Research (CPTEC/INPE: <http://tempo.cptec.inpe.br/boletimtecnico/pt>) that used information of numerical model, modern observation systems, automatic weather stations, satellite and radar images, reanalysis data and regional atmospheric models, such as the Brazilian Global Atmospheric Model and ETA model. The weather systems (fronts, instabilities, and low pressure) were defined according to the synoptic chart and meteorological technical bulletin of the Center for Weather Forecast and Climatic Studies of the National Institute of Space Research (CPTEC/INPE) that used information of numerical models, automatic weather stations, satellite and radar images, reanalysis data and regional atmospheric models, such as the Brazilian Global Atmospheric Model and ETA model.

2.45. Hysplit modelling and Reanalysis data

210 The origin of air masses and moisture transport to the Rio Claro site were evaluated using the HYSPLIT (Hybrid Single Particle Lagrangian Integrated Trajectory) modelling framework (Stein et al., 2015; Soderberg et al., 2013). The trajectories of the air masses were estimated for 240 hours prior to rainfall onset, considering the estimated time of residence of the water vapor (Gimeno et al., 2010, 2020; van der Ent and Tuinenburg, 2017). Start time of trajectories was the same as the start time of rainfall events. The trajectories were computed using NOAA's meteorological data (global data assimilation system, GDAS: 1-degree, global, 2006-present), with ending elevations of the trajectories at 1500 m above the surface, taking into account the climatological height of the Low Level Jet, within 1000-2000 m (Marengo et al., 2004). Ten-day trajectories representing convective events were calculated as trajectory ensembles, each consisting of twenty-seven ensemble members released at start hour of convective rainfall sample collection. Ensembles were produced by varying the initial trajectory wind speeds and pressures, according to the HYSPLIT ensemble algorithm, in order to account for the uncertainties involved in the simulation of individual backward trajectories (Jeelani et al., 2018).

220 Reanalysis data were used to better understand the influence of atmospheric circulation on isotopic composition of rainfall at the study area. ERA-5 climatology (<https://cds.climate.copernicus.eu/cdsapp#!/search?type=dataset>) was used to generate plots of hourly vertical integral of eastward water vapor flux during convective events sampled. The Global Modelling and Assimilation Office (GMAO) data (MERRA-2, 1-hour, 0.5 x 0.625-degree, V5.12.4 <https://goldsmr4.gesdisc.eosdis.nasa.gov/data/MERRA2/M2T1NXFLX.5.12.4/>) were used for calculations of latent heat flux (LHF), and Aqua/AIRS L3 Daily Standard Physical Retrieval (AIRS-only) 1-degree x 1-degree V7.0, Greenbelt, MD, USA; Goddard Earth Sciences Data and Information Services Center (GES DISC) data were used for average outgoing longwave radiation (OLR) (https://disc.gsfc.nasa.gov/datasets/AIRS3STD_7.0/summary). OLR values below $240\text{W}\cdot\text{m}^{-2}$ indicate

230 organized deep convection (Gadgil, 2003). Global Land Data Assimilation System Version 2 (GLDAS-2) Noah Land Surface Model L4 3 hourly 0.25 x 0.25 degree V2.1, Greenbelt, Maryland, USA, Goddard Earth Sciences Data and Information Services Center (GES DISC) were used for calculations of evapotranspiration (https://disc.gsfc.nasa.gov/datasets/GLDAS_NOAH025_3H_2.1/summary). A 10 day mean evapotranspiration values (mm) were computed based on the back hour (240 hours) and coordinates (latitude e longitude) of HYSPLIT trajectories.

235 The origin of air masses and moisture transport to the Rio Claro site were evaluated using the HYSPLIT (Hybrid-Single Particle Lagrangian Integrated Trajectory) modeling framework (Stein et al., 2015; Soderberg et al., 2013). The trajectories of the air masses were estimated for 240 hours prior to rainfall onset, considering the estimated time of residence of the water vapor (Gimeno et al., 2010, 2020; van der Ent and Tuinenburg, 2017). Start time of trajectories was the same as the start time of rainfall events. The trajectories were computed using NOAA's meteorological data (global data assimilation system, GDAS: 1 degree, global, 2006-present), with ending elevations of the trajectories at 1500 m above the surface, taking into account the climatological height of the Low Level Jet, within 1000–2000 m (Marengo et al., 2004). Ten-day trajectories representing convective events were calculated as trajectory ensembles, each consisting of twenty-seven ensemble members released at start hour of convective rainfall sample collection. Ensembles were produced by varying the initial trajectory wind speeds and pressures, according to the HYSPLIT ensemble algorithm, in order to account for the uncertainties involved in the simulation of individual backward trajectories (Jeelani et al., 2018). A sum of the rainfall intensity (mm hr⁻¹) along the trajectories was used to analyse rainout of the moist air masses according to the Jeelani et al. (2018).

240 Reanalysis data were used to better understand the influence of atmospheric circulation on isotopic composition of rainfall at the study area. ERA-5 information was used to evaluate hourly vertical integrals of eastward water vapor flux (kg m⁻¹ s⁻¹) during convective events sampled. The Global Modeling and Assimilation Office (GMAO) data (MERRA-2, 1 hour, 0.5 x 0.625 degree, V5.12.4 were used for calculations of latent heat flux (LHF). Aqua/AIRS L3 Daily Standard Physical Retrieval (AIRS-only) data (1 degree x 1 degree V7.0, Greenbelt, MD, USA, Goddard Earth Sciences Data and Information Services Center) (known as GES DISC) were used for average outgoing longwave radiation (OLR). OLR values below 240 W m⁻² indicate organized deep convection (Gadgil, 2003).

2.56 Identification of convective rainfall events

255 In general, identification of convective precipitation systems was based on the vertical structure of the given precipitation system (lack of the melting layer and bright band –BB) in the radar profiles featuring high reflectivity values ($Z > 38$ dBZ) (Houze, 1993, 1997; Steiner and Smith, 1998; Rao et al., 2008; Mehta et al., 2020; Endries et al., 2018) and satellite imagery (Vila et al., 2008; Ribeiro et al., 2019; Siqueira et al., 2005; Machado et al., 1998). Consequently, convective rainfall was defined in this study by (i) convective cloud nuclei observed in GOES 16 imagery, (ii) no BB detected, (iii) $Z > 38$ dBZ near to the surface and (iv) rainfall intensity (AWS) of at least 10mm.h⁻¹ (Klaassen, 1988) (Fig. 1c,d). The convective nuclei were

Código de campo alterado

Código de campo alterado

260 identified using GOES-16 imagery, determined as a contiguous area of at least 40 pixels with BT lower than 235K ($\leq -38^{\circ}\text{C}$)
 over Rio Claro station, according to previous studies (Ribeiro et al., 2019). In general, identification of convective precipitation
 systems was based on the vertical structure of the given precipitation system (lack of the melting layer and bright band - BB)
 in the radar profiles featuring high reflectivity values ($Z_c > 38$ dBZ) (Houze, 1993, 1997; Steiner and Smith, 1998; Rao et al.,
 2008; Mehta et al., 2020; Endries et al., 2018) and satellite imagery (Vila et al., 2008; Ribeiro et al., 2019; Siqueira et al., 2005;
 Machado et al., 1998). Consequently, convective rainfall was defined in this study by (i) convective cloud nuclei observed in
 265 GOES-16 imagery, (ii) no BB detected, (iii) $Z_c > 38$ dBZ near to the surface and (iv) rainfall intensity (AWS) of at least 10
 mm h^{-1} (Klaassen, 1988) (Fig. 1c,d). The convective nuclei were identified using GOES-16 imagery, determined as a
 contiguous area of at least 40 pixels with BT lower than 235K ($\leq -38^{\circ}\text{C}$) over Rio Claro station, according to previous studies
 (Ribeiro et al., 2019).

2.6 Preliminary assessment of local processes

270 Below-cloud atmospheric conditions are known to be relevant and while we acknowledge that a more robust dataset is required
 to provide sound conclusions, a preliminary assessment of this factor is herein included.

Since the isotopic composition of near-ground water vapor during the rainfall events was not measured, the framework
 proposed by Graf et al. (2019) for interpreting below-cloud effects on rainfall isotopes cannot be applied here. A semi-
 quantitative evaluation of those effects is demonstrated for all rainfall events, despite the need for a more substantial dataset
 275 to establish firm conclusions. This analysis considers the following assumptions: (i) median values of isotope and
 meteorological parameters recorded for each analysed event (Table 1) will be used in the calculations, (ii) linear interpolation
 of air temperature and relative humidity between the cloud base level and the ground level will be adopted to estimate the
 relative humidity at the cloud base (RH_{INT}), (iii) it will be assumed that atmosphere is saturated with water vapour at the cloud
 base level ($\text{RH} = 100\%$), and (iv) the reservoir of water vapour below the cloud base level is isotopically homogeneous (Risi
 280 et al., 2019; Sarkar et al., 2023).

Isotopic evolution of raindrops falling through unsaturated humid atmosphere beneath the cloud base level will be
 calculated using the generally accepted conceptual framework for isotope effects accompanying evaporation of water into a
 humid atmosphere (Craig and Gordon, 1965; Horita et al., 2008). Isotopic evolution of an isolated water body (e.g. falling
 raindrop) evaporating into a humid atmosphere can be described by the following equations (Gonfiantini, 1986):

$$285 \quad \delta = \left(\delta_o - \frac{A}{B} \right) F^B + \frac{A}{B} \quad (1)$$

where

$$A = \frac{h_N \delta_A + \varepsilon_{kin} + \varepsilon_{eq} / \alpha_{eq}}{1 - h_N + \varepsilon_{kin}} \quad (2)$$

and

$$B = \frac{h_N - \varepsilon_{kin} - \varepsilon_{eq} / \alpha_{eq}}{1 - h_N + \varepsilon_{kin}} \quad (3)$$

Parameter F describes the remaining fraction of the evaporating mass of water (raindrop), while δ_A stands for the isotopic composition of ambient moisture. Initial and actual isotopic compositions of the evaporating water body, expressed in δ notation, are represented by δ_0 and δ , respectively. The variables in equations (3) and (4) are described as:

h_N – relative humidity of the ambient atmosphere, normalized to the temperature of the evaporating water body;

α_{eq} – temperature-dependent equilibrium fractionation factor, derived from empirical equations proposed by Horita and Wesolowski (1994);

$$\varepsilon_{eq} - \text{equilibrium fractionation coefficient; } \varepsilon_{eq} = \alpha_{eq} - 1 \quad (4)$$

$$\varepsilon_{kin} - \text{kinetic fractionation coefficient; } \varepsilon_{kin} = \alpha_{kin} - 1 \quad (5)$$

The kinetic fractionation coefficient is a linear function of the relative humidity deficit in the ambient atmosphere (Gat, 2001; Horita et al., 2008):

$$\varepsilon_{kin} = n \cdot \varepsilon_{diff} (1 - h_N) \quad (6)$$

where n describes a turbulence parameter, varying from zero to one and ε_{diff} is the kinetic fractionation coefficient associated with diffusion of water isotopologues in air.

The value of n is controlled mainly by wind conditions prevailing over the evaporating surface. It quantifies the apparent reduction of ε_{diff} due to the impact of turbulent transport. The value of $n = 0.5$, was adopted in the calculations, following the results of laboratory experiments with evaporation of water drops in a humid atmosphere reported by Stewart (1975). Following this same publication, the value of the F parameter for each event was computed based on the rate of change of evaporated drop radius as a function of ambient relative humidity (Stewart, 1975). Droplets with a drop size distribution of 1mm are assumed based on previous studies in this region of study (Zawadzki and Antonio, 1988; Cecchini et al., 2014). Travel time of raindrops drops from the cloud base to the surface was derived from the position of LCL level and the terminal velocity of drops. It was further assumed in the calculations that the difference between drop temperature and ambient air temperature is small, thus allowing to use ambient humidity instead to normalized humidity. Although this assumption may result in an over-estimation of the impact of partial evaporation of raindrops on their isotope characteristics, the effect is expected to be small due to high ambient relative humidities (> 90 %) used in the calculations.

2.7 Statistical tests

The Shapiro-Wilk test was applied to verify that the data distribution was normal (parametric) or non-normal (non-parametric) (Shapiro, S. S.; Wilk, 1965). A significant difference (p -value < 0.05) indicates a non-parametric distribution. A Spearman rank correlation test was used for nonparametric distribution data, whereas Pearson's linear correlation test was applied for parametric data. Correlation tests were conducted between isotopes ($\delta^{18}\text{O}$ and d -excess) and meteorological data (AWS and MRR variables) during the same time interval and from individual events. Correlation tests were not applied to GOES-16 BT

320 and reanalysis data due to their temporal resolution, which reduced the number of samples. All tests were performed with significance levels defined by a p-value < 0.05, using the R statistical package (R Core Team, 2023).

325 A statistical analysis was carried out to characterize regional and local influences, in accordance with He et al. (2018). The initial isotope data of the events (δ_{initial}) closely reflects the initial air mass or vapor from which the precipitation originates. The δ_{initial} and median (δ_{med}) values were employed to identify regional influences in inter-event analysis. Also, the difference ($\Delta\delta$) between the lowest $\delta^{18}\text{O}$ and the highest $\delta^{18}\text{O}$ value represents the local change in δ -value during the intra-event (Muller et al., 2015; He et al., 2018).

3 Results and Discussion

330 A complete database comprising the results of high frequency sampling of convective rainfall events occurring during the study period at the Rio Claro site (isotope characteristics of rainfall as well as selected meteorological parameters characterizing these events) can be found at: (dos Santos et al., 2023). Table 1 contains median values of isotope and meteorological parameters for the studied rainfall events, separated into night time and day time categories.

3.1 Seasonal variations of isotope characteristics and selected meteorological parameters of monthly rainfall

335 Seasonal variations of the isotopic composition of monthly cumulative precipitation and selected meteorological parameters (latent heat flux, outgoing longwave radiation flux (OLR), monthly amount of rainfall) recorded at the Rio Claro site during the study period (September 2019–February 2021), are presented in Fig. 2. The monthly values of meteorological parameters were split in Fig. 2 into day and night fraction. Superimposed on monthly values of $\delta^{18}\text{O}$ presented in Fig. 2a are monthly averages of this parameter derived from high frequency sampling of the convective events. Although they do not cover uniformly the presented study period, it is clear that they follow the seasonal variations of $\delta^{18}\text{O}$ derived for monthly cumulative precipitation samples. A sharp seasonal contrast in the isotopic composition of rainfall for rainy and dry season (austral summer and winter, respectively) is apparent in Fig. 2a. The Local Meteoric Water Lines (LMWL) for the Rio Claro site based on monthly cumulative and high frequency samples (Fig. 3) cannot be directly compared because of incomplete coverage of rainfall in the given month by the high frequency sampling. The high frequency sampling strategy employed in the study was aimed to capture specific rainfall events for each season (cf. Fig. 2a).

345 The seasonal and day-night fluctuations of convective activity characterized by latent heat flux and OLR flux (Fig. 2b,e) and rainfall amount (Fig. 2d) were observed during the study period, resulting in different conditions for occurrence of convective events and high frequency sampling of rainfall. Contrary to summer, during autumn and spring, latent heat fluxes

Formatado: Recuo: Primeira linha: 0 cm

were lower (Fig. 2b) and OLR was higher (Fig. 2c), which in turn may have inhibited convective development related to thermal forcings (Houze, 1997, 1989).

3.1 Isotopic and synoptic characteristics

The isotopic composition of monthly rainfall exhibits clear seasonal variations between September 2019 and February 2021 (Fig. 2a). Seasonal variability was characterized by wet (low $\delta^{18}\text{O}$) and dry (high $\delta^{18}\text{O}$) seasons (austral summer and autumn-spring, respectively). High-frequency sampling of convective events could not be done uniformly during the study period, but it is still evident that median $\delta^{18}\text{O}$ values of high-frequency sampling events (black symbols in Fig. 2a) follow the seasonal isotope variability.

The summer months were characterized by the influence of convective activity, reflected in high latent heat flux and lower OLR (Fig. 2c). During autumn and spring, significant lower latent heat flux and higher OLR were associated with less convective development (Houze, 1997, 1989). The formation of convective rainfall may not be primarily controlled by diurnal thermal convection, as rainfall is more likely to be associated with frontal systems (Siqueira and Machado, 2004), as observed in the rainfall episodes during autumn and spring.

A significant influence of the cold fronts was observed before, during, and after their passage over the study area (Fig. 2a). During autumn and spring, the convective events of 2019/11/05, 2020/11/18, and 2020/05/23 were associated with cold fronts in the study area. On 2020/06/09, changes in the regional atmosphere over the state of São Paulo caused convective rainfall due to an instability (frontal) system resulting from a cold front settling over the southern region of Brazil. During the summer season, convective rainfall also occurred on 2020/02/01 and 2021/02/24 due to cold fronts and instability (frontal), respectively. In addition, the thermal convection of the continental region caused atmospheric ascent via surface heating in the inland of Brazil, leading to a system responsible for the convective rainfall event on 2020/01/30. As a result of the interaction between thermal convection and the incursion of the frontal system, a low-pressure system (frontal) was responsible for the convective rainfall event on 2020/02/10.

Table 1 presents an overview of the sampling, isotope parameters (δ_{initial} , δ_{med} , $\Delta\delta$) and median values of meteorological variables from individual events. Sampled events had a duration of 141 or fewer minutes. The T and Twd exhibited small differences among the events. In contrast, RR, RH, LCL, Zc, w, and BT varied considerably between events. The maximum recorded values for these parameters were 97 %, 489 m, 46 dBZ, 8 m s⁻¹ and -63 °C, respectively.

Isotope values varied among convective events, with a range of -11.0 ‰, -92.8 ‰ and +15.7 ‰ for median values of $\delta^{18}\text{O}$, $\delta^2\text{H}$ and d -excess, respectively. The maximum differences between the δ_{initial} and δ_{med} for $\delta^{18}\text{O}$, $\delta^2\text{H}$, and d -excess were 1.6 ‰, 9.1 ‰, and 9.5 ‰, respectively. The maximum $\Delta\delta$ values for all isotopes parameters, $\delta^{18}\text{O}$, $\delta^2\text{H}$ and d -excess were 7.3 ‰, 43.0 ‰ and 19.2 ‰, respectively.

3.2. Inter-event variability of the isotope parameters

Hysplit air mass back-trajectories revealed three main locations as moisture origin during the presence of convective rainfall: Amazon forest, Atlantic Ocean, and southern Brazil (Fig. 3). The sourcing of moisture for rainfall over Rio Claro varies seasonally and spatially, suggesting complex interactions in moisture transport and mixing that strongly influence the initial isotopic composition of rainfall throughout the year (Table 1).

Summer rainfall events were characterized by the trajectory and length of moist air masses arriving from the Amazon forest (2020/02/10, 2020/02/01, and 2020/01/30) (Fig. 3a). As a result, there was a large amount of rainfall along Hysplit trajectories. Rainfall amounts were 177 mm, 126 mm and 78 mm, respectively, for these dates. Remarkably, these events exhibited very similar isotope characteristics ($\delta^2\text{H}_{\text{initial}}$, $\delta^{18}\text{O}_{\text{initial}}$) (Table 1). In contrast, the event on 2021/02/24 presented higher δ_{initial} values, reflecting the oceanic moisture influence (Fig. 3a), with a lowest amount of rainfall (53 mm) along Hysplit trajectory.

Based on ERA-5, the vertically integrated eastward vapor flux corroborates the influence of a distinct mechanism for moisture transport and δ_{initial} values. Negative values for vertical vapor fluxes over the Amazon forest during sampled convective events in summer (Fig. 4a, b, d) clearly illustrate a westward moisture flux from the Atlantic Ocean to the Amazon forest. Positive values in the central-southern region of Brazil indicate moisture being transported eastward from the Amazon forest. However, these moisture fluxes were not observed on 2021/02/24 when the eastward vapor flux was positive with high values over the Atlantic Ocean (250 ~ 750 $\text{kg m}^{-1} \text{s}^{-1}$).

The autumn convective events on 2020/05/23 and 2020/06/09 revealed a significant continental origin of moist air masses (from south-western Brazil). In addition, during the second event, the Amazon-type trajectory started in the southern Atlantic and did not reach the boundary of the rainforest (Fig. 3b). In both autumn events, there was the lowest amount of rainfall (4 mm) along Hysplit trajectories. On 2020/05/23 negative vertical flux values (-500 ~ -250 $\text{kg m}^{-1} \text{s}^{-1}$) were observed in south-western Brazil, indicating moisture transport from the Atlantic Ocean to the continent. This favored a vapor flux (500 ~ 750 $\text{kg m}^{-1} \text{s}^{-1}$) from western Brazil to the study area (Figure 4f). On 2020/06/09, there were slightly negative values (-250 ~ 0 $\text{kg m}^{-1} \text{s}^{-1}$) of eastward vapor flux in the Amazon forest, indicating less influence from rainforest moisture. Conversely, positive vapor flux values (250 ~ 500 $\text{kg m}^{-1} \text{s}^{-1}$) were observed in the western part of continental Brazil.

Two events in the spring season (Fig. 3c) also showed contrasting origin of moisture and initial d -excess values, despite only slight differences in $\delta^{18}\text{O}_{\text{initial}}$ (Table 1). The mean trajectory on 2020/11/18 clearly belongs to the Amazon category, although it only passed over the south-eastern boundary of the Amazon rainforest and had a much shorter length and lower rainfall along Hysplit trajectory (23 mm) compared to the Amazon trajectories observed during the summer season. Thus, positive values of the eastward vapor flux (250 ~ 750 $\text{kg m}^{-1} \text{s}^{-1}$) were not distributed along the Amazon forest to the Atlantic Ocean as typically observed (Fig. 4h). The mean trajectory on 2019/11/05 the eastward vapor flux (> 500 $\text{kg m}^{-1} \text{s}^{-1}$, Fig. 4g) were circling around Rio Claro, indicating the continental moisture origin (from southern Brazil), and low amount of rainfall along Hysplit trajectory of 8 mm.

3.2 Intra-event variability of the isotope and meteorological parameters

Temporal evolution of isotope characteristics ($\delta^{18}\text{O}$, d -excess) and selected meteorological parameters (brightness temperature, MRR-reflectivity and rainfall amount) of convective rainfall events sampled and analyzed in this study is presented in Fig. 4.

In this figure, radar eos for all sampled events. The emphasizes the absence of pattern in measured values for the reflectivity (Z_e) on the vertical profile (Fig. 4a-b, g-h, m-n, s-t), only near surface higher values were observed (from 2km to 200m), indicating an increase in raindrop size, hence an increase in Z -values and rain rates. Despite the similar vertical structure, the temporal evolution was quite distinct between the events, according to the season when the event was collected. The brightness temperature of GOES-16 (BT) has distinct temporal distributions between events (Fig. 4e-f, k-l, q-r, w-x); despite the no relationship observed between variations of BT and a change in isotope values.

For the events collected during the summer, 2020/02/01-day (Fig. 4c,e) and 2020/01/30-night (Fig. 4d,f) the duration were similar (20min and 25min, respectively), similar temporal $\delta^{18}\text{O}$ evolution (-10.29 — -10.07% (stationary trend) and -10.13 — -9.91% (little increasing trend) and similar rain rates trends (2.8 — 0.1mm and 4.4 — 0.1mm), respectively. Contrary to the 2021/02/24 day (Fig. 4i, k) and 2020/02/10 night (Fig. 4j, l) events, that had similar longer duration (02h01min and 02h39min, respectively), however, had distinct variations of $\delta^{18}\text{O}$ and rain rates (-7.60 — -4.47% (increasing trend) and -12.35 — -13.99% (decreasing trend) and 2.6 — 0.3mm and 0.6 — 0.6mm , respectively), illustrate the remarkably difference between day (enriched) and night (depleted) isotopic composition. Lower d -excess values were observed on 2021/02/24 (9.3 — -1.2%) 2020/02/01 (11.3 — -7.0%) and 2020/02/10 (21.4 — -4.8%). While for 2020/02/01 and 2020/02/10 these lower d -excess values have been observed at the end of event, when rain rates were lower (0.01mm and 0.8mm , respectively), indicating the residual precipitation, as the rainfall dissipates (Celle Jeanton et al., 2004), on 2021/02/24 lower d -excess values were observed in some parts of the event, associated to lower Z -values (from 16:38 to 17:15). The differences on isotopic composition and a possible effect to below-cloud evaporations for these events are detailed discussed in section 3.4.

For the events collected during the autumn (2020/06/09 (Fig. 4o) and 2020/05/23 (Fig. 4p) values and variations on $\delta^{18}\text{O}$ were similar (-3.67 — -2.76% and -2.67 — -2.75%), the first event showed a little decreasing trend, while the second is stationary. On the other hand, 2020/06/09 and 2020/05/23 d -excess values (25.4 — 6.3% and 16.7 — 19.0% , respectively); trends (w-shaped and stationary), RR (6.2 — 0.01mm and 2.6 — 0.2mm), BT (-55 — -35°C and -60 — -52°C) and vertical structure variable (two peaks of higher Z -values near surface (4m) and one peak on high Z -values at start (Fig. 4n), respectively). Despite the decrease of BT values along the time observed in the 09/06/2020 event, lower d -excess values and a slight $\delta^{18}\text{O}$ increase have been observed during the peak of RR. These changes on isotope distribution could be related to the passage of convective development zones during the event evolution (Risi et al., 2010), from a strong convective activity, corroborated by lower BT values (-55 — -52°C) and higher Z (between 17:04 and 14:44), to convection transition activity, represented by an increase on BT (-51 — -48°C) and lower Z (between 17:46 to 18:09) and finally, to lower convective development, characterized by higher BT values ($> 45^\circ\text{C}$), and higher Z (between 18:12 to the end).

445 Spring convective events, collected on 2019/11/05 (Fig. 4u,) and 2020/11/18 (Fig. 4v), have shown opposite isotope
variations (-3.00 ~ -1.78‰ and -2.76 ~ -5.40‰) and trends (increasing and decreasing, respectively). Values of RR, normally
higher, BT, normally lower, did not present relationship with the isotopic variation (Fig. 4w, x). Values of d excess were
stationary on 2019/11/05 event (28.0 ~ 21.0‰), while presented an increase trend during the event collected on 2020/11/18
(10.2 ~ 23.1‰). Any value of d excess were lower than 10‰. The vertical profile of Z is quite distinct between spring events
(Fig. 4s, t), higher Z values near surface was observed at the start and lower at the end of 2019/11/05, while on 2020/11/18 a
450 strong peak of Z occurred at the end (between 16:15 and 16:25). These temporal evolutions in the vertical profile of events
2019/11/05 and 2020/11/18 illustrate the opposite isotope trends (increasing and decreasing, respectively) generally related to
the fast condensation and rainfall formation due to the strong updrafts (e.g. Sodemann, 2006; Gedzelman and Lawrence, 1990)
and isotopic equilibrium between droplets and vapor (e.g. Celle-Jeanton et al., 2004; Barras and Simmonds, 2009; Muller et
al., 2015), respectively.

455 The weather systems (indicated for each rainfall event in Fig. 6) interacting with the moisture available producing the
rainfall systems. A large influence of the cold fronts was observed before, during and after their passage over the study area.
Convective rainfall directly formed by the frontal systems (cold front acting at the study area) for 2019/11/05, 2020/11/18,
2020/05/23 and 2020/02/01 events had distinct isotope trends (increasing, decreasing, stationary and stationary), respectively.
The instability (frontal) system (when a cold front is localized in the south of Brazil and generates changes in the regional
460 atmosphere over São Paulo state) occurred for 2020/06/09 (decreasing) and 2021/02/24 (increasing trend) events, while
thermal instability formed by atmospheric ascend due to surface heat in inland Brazil of 2020/01/30 (little increasing trend),
and low pressure (frontal) system (when the cold front is localized in the Atlantic Ocean near Southeast portion of Brazil and
interacts with regional atmosphere) for 2020/02/10 (decreasing trend).

465 The large diversity of trends is quite different observed in previous studies of cold fronts in mid-latitudes, generally related
to the V-shaped and strong δ depletion (e.g. Aemisegger et al., 2015; Gedzelman and Lawrence, 1990; Celle-Jeanton et al.,
2004; Muller et al., 2015). Apparently, for intra-events presented here, it is difficult to relate the contribution of weather
systems control of isotopic variability, due to the different conditions of temperature, moisture available and convective activity
(lower during autumn-spring and higher during summer in Fig. 2) along the seasons. Perhaps, which contributes to connecting
regional processes to isotope variations, mainly the large d -excess distributions, is the associate origin and transport with inter-
470 event evaluation, illustrated in Fig. 5 and 6 detailed in the 3.3. section.

3.3 Intra-event variability of the isotope and meteorological parameters

The temporal evolution of isotope characteristics and selected meteorological parameters of convective rainfall are shown in
Fig. 5 (summer) and Fig. 6 (autumn-spring). The study emphasizes the lack of pattern in the measured values for reflectivity
(Zc) in the vertical profile. Only higher Zc values were observed near the surface (from 2km to 200m), which indicates an

475 [increase in rain rates. Despite the similar vertical structure, the temporal evolution varied considerably among events. Furthermore, the GOES-16 BT shows unique temporal patterns among events.](#)

[The differences in \$\Delta\delta\$ observed between convective events were explained by intra-events \(refer to Table 1\) and how local factors may affect the regional isotopic signature as illustrated by the inter-event analysis.](#)

[3.3.1. Summer intra-events](#)

480 [Lower values of \$\Delta\delta^{18}\text{O}\$ were observed on the 2020/02/01 and 2020/01/30 compared to higher \$\Delta\delta^{18}\text{O}\$ values observed on the 2020/02/10 and 2021/02/24. In contrast, all summer events exhibit high \$\Delta\delta\$ values for \$d\$ -excess \(Table 1\). Despite this variation in isotopic amplitude, the evolution of these events is characterized by different amounts of available humidity \(Table 1 and Table 2\). For the 2021/02/24 event, lower humidity values were observed below the cloud \(\$\text{RH}_{\text{INT}} = 93\%\$ \) and at the surface \(\$\text{RH} 78 \sim 88\%\$, median value \$86\%\$ \). The other events had higher humidity conditions \(\$\text{RH}_{\text{INT}} = > 96\%\$ and \$\text{RH} > 90\%\$ \).](#)
485 [Nevertheless, only 2021/02/24 and 2020/02/10 show \$d\$ -excess values lower than \$10\text{‰}\$, suggesting that the specific local factors can influence the variations in the isotopic composition of the precipitation, as shown below for each event.](#)

[Specifically, the events on 2020/02/01 \(Fig. 5c,e\) and 2020/01/30 \(Fig. 5d,f\) showed consistent \$\delta^{18}\text{O}\$ trends \(\$-11.6 \sim -10.0\text{‰}\$ and \$-10.6 \sim -9.6\text{‰}\$, respectively\). In contrast, these events showed an inverted V-shaped \(from \$11.3 \sim 15.3\text{‰}\$ to \$15.4 \sim 7.0\text{‰}\$ \) and V-shaped \(from \$20.8 \sim 11.4\text{‰}\$ to \$14.6 \sim 16.2\text{‰}\$ \) patterns for \$d\$ -excess, respectively. The patterns of rainfall intensity were similar for both events, with high rainfall amount at the beginning of event, decreasing over the time. In BT values, decreased \(\$-50 \sim -65\text{ °C}\$ \) and constant variations \(\$-52 \sim -53\text{ °C}\$ \) occurred on 2020/02/01 and 2020/01/30 events, respectively. The strong and significant \(\$p < 0.0001\$ \) correlations were observed between isotopic composition and MRR parameters for 2020/02/01: \$\delta^{18}\text{O}\$ -Zc \(\$r = -0.9\$ \), \$\delta^{18}\text{O}\$ -w \(\$r = -0.9\$ \), \$d\$ -excess-Zc \(\$r = 0.9\$ \) and \$d\$ -excess-w \(\$r = 0.9\$ \), while there were no correlations between isotopic composition and meteorological parameters for 2020/01/30.](#)

495 [On 2021/02/24 \(Fig. 5i,k\) and 2020/02/10 \(Fig. 5j,l\), notable fluctuations were observed in both the isotope and meteorological parameters. On 2021/02/24, \$\delta^{18}\text{O}\$ varied from \$-7.9 \sim -4.4\text{‰}\$, and \$d\$ -excess varied from \$1.2\$ to \$18.4\text{‰}\$. The evolution of the event was characterized by varying local weather conditions, as evidenced by a larger BT range \(\$-38 \sim -57\text{ °C}\$ \). Radar reflectivity is displayed in a vertical profile, illustrating these changes, with larger Zc values during the event \(red colors in Fig. 5g\). As a result, three peaks of maximum rainfall amount were observed, which corresponded to the distinct](#)
500 [\$\delta^{18}\text{O}\$ and for \$d\$ -excess values: at 15:49 local time \(\$2.6\text{ mm}\$, \$-7.6\text{‰}\$ and \$13.0\text{‰}\$ \), at 16:24 \(\$3.1\text{ mm}\$, \$-6.9\text{‰}\$ and \$8.4\text{‰}\$ \) and at 17:28 \(\$3.3\text{ mm}\$, \$-7.9\text{‰}\$ and \$17.9\text{‰}\$ \), respectively. Also, strong, and significant \(\$p < 0.05\$ \) correlation was observed between \$\delta^{18}\text{O}\$ -R \(\$r = -0.8\$ \), \$d\$ -excess-R \(\$r = -0.6\$ \) and MRR parameter, \$\delta^{18}\text{O}\$ -Zc \(\$r = -0.6\$ \) and \$d\$ -excess-Zc \(\$r = -0.5\$ \).](#)

[On 2020/02/10, \$\delta^{18}\text{O}\$ showed a variation from \$-15.2 \sim -7.9\text{‰}\$ and for \$d\$ -excess from \$4.8 \sim 21.4\text{‰}\$. During the beginning of the event and until 21:03 local time, high BT values \(\$-16 \sim -45\text{ °C}\$ \) corresponded to the higher Zc values \(red colors in Fig. 5h\) and high RH \(\$\sim 97\%\$ \). After this time, lower Zc and lowest BT values were observed \(\$-45 \sim -57\text{ °C}\$ \). There were two](#)

breakpoints in the rainfall trend (increasing to decreasing) corresponding to the change in isotope values ($\delta^{18}\text{O}$ and d -excess), occurring at 20:36 (4.8 to 3.2 mm, -13.9 to -9.5 ‰ and 15.7 to 9.4 ‰) and 21:57 (2.0 to 0.8 mm, -14.9 to -7.9 ‰ and 21.4 to 4.8‰) respectively. In addition, for this event strong and significant ($p < 0.05$) correlation was observed only between $\delta^{18}\text{O}$ -RH ($r = -0.5$) and d -excess-RH ($r = 0.5$).

510 3.3.2 Autumn and spring intra-events

Lower $\Delta\delta^{18}\text{O}$ values were observed during autumn and spring events in comparison to summer events. Both autumn and spring events showed higher $\Delta\delta$ values for d -excess when compared to summer events. For the events on 2020/05/23 ($\text{RH}_{\text{INT}} = 93\%$, RH 78 ~ 89 %, with median of 87 %) and 2020/11/18 ($\text{RH}_{\text{INT}} = 92\%$ and RH 70 ~ 90 %, with median of 85 %), lower humidity conditions were recorded, whereas for all other events, humidity conditions were high ($\text{RH}_{\text{INT}} = > 97\%$ and RH = > 90%) as show in Tables 1 and 2.

For autumn events on 2020/06/09 (Fig. 6a,c,e) and 2020/05/23 (Fig. 6b,d,f), a slight increase trend (-3.7 ~ -1.5‰) and stationary trend (-2.6 ~ -2.7‰) were observed regarding $\delta^{18}\text{O}$. On the other hand, for the same events, d -excess showed a W-shaped trend (17.7 ~ 6.3 ‰, during the last part of the event) and V-shaped pattern (16.7 ~ 19.0 ‰), respectively. Both events demonstrated a decrease in rainfall amount: from 6.2 to 0.2 mm on 2020/06/09, 2020, and from 2.6 to 0.2 mm on 2020/05/23. Additionally, the range of BT increased from -55°C to -35 °C and from -60°C to -52 °C, respectively. Strong and significant ($p < 0.05$) correlations were observed between isotopic and surface meteorological parameters during the event on 2020/06/09, $\delta^{18}\text{O}$ -RH ($r = 0.5$), $\delta^{18}\text{O}$ -T ($r = -0.6$), d -excess-RH ($r = -0.6$), and d -excess-T ($r = 0.7$). However, no significant correlations were found during the event on 2020/05/23.

Spring convective events exhibited contrasting variations in isotopes and meteorological conditions. On 2019/11/05 (Fig. 6g,i,k), slight fluctuations were observed in $\delta^{18}\text{O}$ (-3.0 ~ -1.7 ‰, slightly increasing-trend), while d -excess values were higher (21.0 ~ 28.0 ‰, decreasing trend). This slight fluctuations in $\delta^{18}\text{O}$ values correspond to the constant and higher Z_c near surface. This is evidenced by the highest and significant ($p < 0.0003$) correlations observed between isotopic and MRR parameters, $\delta^{18}\text{O}$ - Z_c ($r = -0.7$), $\delta^{18}\text{O}$ -w ($r = -0.7$), and d -excess-w ($r = 0.6$). In contrast, these fluctuations were not related with changes in rainfall amount (0.6 ~ 5.0 mm) and BT (-65 ~ -62 °C).

On 2020/11/18, two distinct steps revealed a decreasing trend in $\delta^{18}\text{O}$ (-2.7 ~ -5.4 ‰), and a substantial increasing trend in d -excess (10.2 ~ 23.1 ‰) (Fig. 6h,j,l). Between 15:10 and 16:05 local time, the vertical profile of the MRR exhibited variable Z_c values, with concomitant decreases in both BT values (-62 and -65 °C) and $\delta^{18}\text{O}$ (-2.7 ~ -4.0 ‰) and increase in both rainfall (1.2 ~ 2.0 mm), d -excess (10.2 ~ 19.6 ‰) and RH (70 ~ 82 %) values. After this period, Z_c values increased closer to the surface, resulting in a slight decrease in temperature (-65 ~ -63 °C). Additionally, $\delta^{18}\text{O}$, d -excess, rainfall amount and RH fluctuated (-3.8 ~ -5.4 ‰, 18.0 ~ 23.1 ‰, 1.8 ~ 2.2 mm and 84 ~ 90 %, respectively). Regardless of this, no significant correlations were found due to the considerable variations between isotopic and rainfall, as well as BT and MRR parameters.

The significant ($p < 0.001$) correlations were only observed for $\delta^{18}\text{O-RH}$ ($r = -0.9$), $\delta^{18}\text{O-T}$ ($r = 0.9$), d -excess-RH ($r = 0.9$), and d -excess-T ($r = -0.9$).

3.3. Inter-event variability of the isotope and meteorological parameters

Figure 5 shows Hysplit ensemble trajectories calculated for each analyzed rainfall event, divided into seasons (summer, autumn and spring). It is clear from Table 1 and Fig. 5 that three summer events, undoubtedly associated with moist air masses arriving from the Amazon basin (2020/02/10, 2020/02/01 and 2020/01/30), have remarkably similar isotope and meteorological characteristics ($\delta^2\text{H}$, $\delta^{18}\text{O}$, d excess, RH), irrespectively whether they are day time or night time events. In contrast, the day time event which occurred on 2021/02/24 and revealed higher δ values, lower d excess and lower relative humidity, was fed by moisture of Atlantic origin (Fig. 5a).

The estimated vertical integral eastward vapor fluxes using data from ERA-5 (Fig. 6) combined with Hysplit air masses backward trajectories, shows clearly the predominant influence of Amazon moisture for 2020/02/01, 2020/01/30 and 2020/02/10 convective events, representing summer events (Fig. 6a, b, d), marked by the negative values for vertical vapor fluxes ($< -250 \text{ kg m}^{-1}\text{s}^{-1}$) over the Amazon basin (indicating the direction of moisture vapor flux from the Ocean to Amazon Forest) and positive values ($> 500 \text{ kg m}^{-1}\text{s}^{-1}$) over the central-southern portion of Brazil (indicating the direction of vapor flux from Amazon basin with pathways over the study area to the Atlantic Ocean). The higher positive values ($\sim 750 \text{ kg m}^{-1}\text{s}^{-1}$) in red color in Figure 6a, b, d illustrate the acts of cold fronts between the continental portion and the Atlantic Ocean. This regional pattern was not observed during on 2021/02/24, eastward vapor flux is positive and has high values over the Atlantic Ocean ($250 \sim 750 \text{ kg m}^{-1}\text{s}^{-1}$), corroborating the distinct moisture transport, δ values and relative humidity values.

The two events representing autumn season (2020/05/23—night time event and 2020/06/09—day time event) were associated with mean trajectories similar to those calculated for the spring season (Fig. 5b). In this case the continental origin of moist air masses (south-western Brazil) is more pronounced (2020/05/23), whereas the Amazon-type trajectory starts in southern Atlantic and does not reach the boundary of the rainforest. In Fig. 6, the eastward vapor flux illustrates the continental origin of moist air masses on 2020/05/23 and Atlantic origin for the 2020/06/09. While on 2020/05/23 negative values ($-500 \sim -250 \text{ kg m}^{-1}\text{s}^{-1}$) were observed in south-western Brazil (indicating transport from the Atlantic Ocean to the continent), which formed a vapor flux of positive values ($500 \sim 750 \text{ kg m}^{-1}\text{s}^{-1}$) from western Brazil to the study area (Figure 6f), on 2020/06/09 slight negative values ($-250 \sim 0 \text{ kg m}^{-1}\text{s}^{-1}$) of eastward vapor flux over Amazon basin indicate the decrease of rainforest moisture flux, positive vapor flux values ($250 \sim 500 \text{ kg m}^{-1}\text{s}^{-1}$) over the western portion of continental Brazil and study area corroborate that the trajectory started from Atlantic Ocean to arrive directly over the Rio Claro station (Fig. 5b and Fig. 6e).

Finally, two day-time events available for the spring season (Fig. 5c) also reveal contrasting origin of moisture. The mean trajectory for the 2020/11/18 belongs clearly to the Amazon category, although it is passing only over the south-eastern boundary of the Amazon rainforest and has much shorter extension when compared with the Amazon trajectories observed during the summer season, thus positive values of eastward vapor flux ($250 \sim 750 \text{ kg m}^{-1}\text{s}^{-1}$) are not distribution along from

Amazon basin to Atlantic Ocean as typically observed previously (Fig. 6h). The mean trajectory for the second event (2019/11/05) and higher positive eastward vapor flux ($> 500 \text{ kg m}^{-1}\text{s}^{-1}$, Fig. 6g) are circling around the Rio Claro, pointing to the continental origin (southern Brazil) of moist air masses responsible for this event.

It is apparent from Fig. 5a and Table 1 that three summer events mentioned above (2020/02/10, 2020/02/01 and 2020/01/30) are very consistent in terms of the length and shape of backward trajectories of moist air masses, as well as isotope characteristics of the rainfall events produced from those air masses. The mean $\delta^2\text{H}$, $\delta^{18}\text{O}$ and d -excess values for those three events are equal -76.6, -11.4, 15.5‰, respectively. The ground level relative humidity is also consistent (mean value 94%, range ca. 5%). Autumn and spring events also reveal remarkable degree of consistency in terms of origin of moisture and isotope characteristics of rainfall (cf. Table 1 and Fig. 5b,c). The mean $\delta^2\text{H}$, $\delta^{18}\text{O}$ and d -excess values are equal -6.4, -3.4, 19.1‰, respectively. Mean relative humidity is equal 90.8%. Those dramatic differences between δ values of convective rainfall sampled during summer months and that sampled during spring and autumn (ca. 8‰ for $\delta^{18}\text{O}$ and 70‰ for $\delta^2\text{H}$), generated under similar thermal conditions in the region, call for explanation. Also, substantially higher mean d -excess value for spring and autumn events (the difference with respect to summer mean value equal 3.6‰) needs to be understood.

We suggest that isotope characteristics of convective events investigated in this study (both the δ values and the d -excess) are controlled by three major factors: (i) the origin of moisture and the degree of rainout of moist air masses responsible for precipitation over the Rio Claro site, (ii) the backward flux of water vapor released by the continent to the regional atmosphere, and (iii) possible modification of isotopic signatures of rainfall due to partial evaporation of raindrops and their interaction with ambient water vapor reservoir below the cloud base.

The overwhelming majority of moist air masses arriving at Rio Claro during summer have their source somewhere in the equatorial Atlantic and are subject to long rainout history extending over several thousand kilometers. Along this pathway those air masses interact with the Amazon rainforest. Intensive recycling of moisture leads to small continental gradient of δ values of rainfall across the Amazon basin (Salati et al., 1979; Rozanski et al., 1993) and elevated d -excess (Gat, J. R., & Matsui, 1991). While arriving at Rio Claro, those air masses are strongly depleted in heavy isotopes due to enhanced rainout over the second portion of their trajectory (after deflection of moist air masses from the Andes), but they maintain the elevated deuterium excess inherited through interaction of maritime moisture with the Amazon rainforest. Such air masses generate precipitation depleted in heavy isotopes, with high d -excess value, as observed over Rio Claro.

The analyzed convective events representing spring and autumn season have substantially shorter 10-day trajectories suggesting that atmospheric "pump" transporting moisture from the equatorial Atlantic to the Amazon basin is much weaker or non-existing during this time of a year. Those short trajectories also suggest enhanced interaction with the surface of the continent. The backward flux of moisture from the surface to the atmosphere, generated in evapotranspiration processes apparently becomes the major source of moisture for rainfall occurring during spring and autumn in the region.

It is a generally accepted fact that transpiration process, at its steady state, is a non-fractionating process i.e. it returns the soil water pumped by the plants to the atmosphere without any discernible change of its isotopic composition (e.g. Cuntz et al., 2007; Flanagan et al., 1991; Dongmann and Nürnberg, 1974). In the study region we have distinct dry and wet period (cf.

Fig.2d). If we assume that soil water accessible to plants has the isotopic characteristics equal to mean values of the four summer events discussed above (68,67, -10,28, 13.5‰, for $\delta^2\text{H}$, $\delta^{18}\text{O}$ and d excess, respectively), than water vapour released to the regional atmosphere in the transpiration process will have the same isotopic signatures. Now, if we assume that this water vapour is lifted up by convection processes and reaches the condensation level, the isotopic composition of the first condensate can be easily calculated assuming isotope equilibrium between gaseous and liquid phase of water at the cloud:

$$\delta_r = \alpha_{eq}(1000 + \delta_v) - 1000 \quad (1)$$

where δ_r and δ_v signify delta-values of liquid (condensate) and vapor phase, respectively, at isotopic equilibrium, whereas α_{eq} stands for equilibrium fractionation factor. Equilibrium fractionation factors for ^2H and ^{18}O were calculated using empirical expressions proposed by (Horita and Wesolowski, 1994). The assumed condensation temperature was equal 18°C (cf. Tdw for spring and autumn events – Table 1). The calculated isotope characteristics of the first condensate are equal +12.2, -0.46 and 15.8‰, for $\delta^2\text{H}$, $\delta^{18}\text{O}$ and d excess, respectively. Large potential of the transpiration process in generation of isotopically enriched rainfall is clearly seen from the above exemplary calculation.

In addition to water vapor generated in the transpiration process, the backward vapor flux from the continent to the regional atmosphere will also include evaporation of surface water bodies located in the footprint area of the rainfall collection site. Evaporation of surface water bodies will generate vapor slightly depleted in heavy isotopes when compared to the source water subject to evaporation, and isotopic composition of this vapor will be located on the Local Evaporation Line (LEL), to the left-hand side of the Local Meteoric Water Line, thus exhibiting high d excess values (e. g. Rozanski et al., 2001). The fact that the mean d excess value of spring and autumn convective rainfall events analyzed in this study (ca. 19.1‰) is higher than that obtained for the mean isotopic composition of four analyzed summer events (ca. 13.5‰—cf. discussion above) provides the evidence that the flux of water vapor to the regional atmosphere, a part of dominating contribution generated by the transpiration process (10-day mean evapotranspiration values of summer, spring and autumn events are equal 41mm, 31mm and 24mm, respectively), will also contain the fraction originating from surface water evaporation in the region.

3.4. Assessing the impact of below-cloud processes on the isotope characteristics of convective precipitation

The third factor which may contribute to the observed large differences between δ values of convective rainfall events sampled during summer months and those collected during spring and autumn, (ca. 8‰ for $\delta^{18}\text{O}$ and 70‰ for $\delta^2\text{H}$), generated under similar thermal conditions in the region, is the possible modification of the isotopic signatures of raindrops due to their partial evaporation and interaction with ambient water vapor reservoir below the cloud base level. This issue will be discussed below in some detail. As the isotopic composition of near-ground water vapour during the sampled rainfall events has not been measured, application of the interpreting framework for below-cloud effects on the isotopic characteristics of rainfall proposed by Graf et al. (2019) cannot be adopted here. Instead, a rough, semi-quantitative assessment of the impact of those effects in the context of the discussed isotope data will be presented below. The assessment will focus on two rainfall events sampled in summer: (i) 2020/02/10 night time event, and (ii) 24/02/2021 day time event.

635 Due to lack of appropriate data, a number of simplifying assumptions has to be made: (i) median values of isotope and meteorological parameters recorded for each analysed event (Table 1) will be used in the calculations, (ii) linear interpolation of air temperature and relative humidity between the cloud base level and the ground level will be adopted, (iii) it will be assumed that atmosphere is saturated with water vapour at the cloud base level (RH = 100%), and (iv) the reservoir of water vapour below the cloud base level is isotopically homogeneous.

640 Isotopic evolution of raindrops falling through unsaturated humid atmosphere beneath the cloud base level will be calculated using generally accepted conceptual framework for isotope effects accompanying evaporation of water into a humid atmosphere (Craig and Gordon, 1965; Horita et al., 2008). Isotopic evolution of an isolated water body (e.g. falling raindrop) evaporating into a humid atmosphere can be described by the following equation (Gonfiantini, 1986):

$$\delta = \left(\delta_a - \frac{A}{B} \right) F^B + \frac{A}{B} \quad (2)$$

645 where

$$A = \frac{h_N \delta_a + \epsilon_{kin} + \epsilon_{eq} / \alpha_{eq}}{1 - h_N + \epsilon_{kin}} \quad (3)$$

and

$$B = \frac{h_N - \epsilon_{kin} - \epsilon_{eq} / \alpha_{eq}}{1 - h_N + \epsilon_{kin}} \quad (4)$$

650 Parameter F signify the remaining fraction of the evaporating mass of water (raindrop) while δ_a stands for the isotopic composition of ambient moisture. Initial and actual isotopic compositions of the evaporating water body, expressed in δ notation, are represented by δ_i and δ , respectively (expressed here as a fractions of unity). The meaning of the remaining parameters in equations (3) and (4) reads as follows:

h_N —relative humidity of ambient atmosphere, normalized to the temperature of the evaporating water body

α_{eq} —temperature dependent equilibrium fractionation factors, derived from empirical equations proposed by Horita and

655 Wesolowski (1994).

ϵ_{eq} —equilibrium fractionation coefficient. $\epsilon_{eq} = \alpha_{eq} - 1$

ϵ_{kin} —kinetic fractionation coefficient. $\epsilon_{kin} = \alpha_{kin} - 1$.

It can be shown (Gat, 2001; Horita et al., 2008) that kinetic fractionation coefficient is a linear function of the relative humidity deficit in the ambient atmosphere:

$$\epsilon_{kin} = n \epsilon_{diff} (1 - h_N) \quad (5)$$

660 where n stands for numerical factor, called turbulence parameter, varying in the range from zero to one, h_N signify relative humidity normalized to the temperature of the evaporating water body, whereas ϵ_{diff} is the kinetic fractionation coefficient associated with diffusion of water isotopologues in air.

665 The value of n is controlled mainly by wind conditions prevailing over the evaporating surface. It quantifies apparent reduction of the diffusive fractionation coefficient ϵ_{diff} due to impact of turbulent transport. The value of $n = 0.5$, was adopted in the calculations, following the results of laboratory experiments with evaporation of water drops in humid atmosphere

670 reported by Steward (1975). The value of F parameter for each analyzed event was assessed based on the same publication (Stewart, 1975) (Fig. 4) assuming drop radius equal 1 mm. Travel time of raindrops drops from the cloud base to the surface was derived from the position of LCL level and the terminal velocity of drops, both reported for the analyzed events in Table 1. It was further assumed in the calculations that the difference between drop temperature and ambient air temperature is small, thus allowing to use ambient humidity instead to normalized humidity. Although this assumption may result in an over-estimation of the impact of partial evaporation of raindrops on their isotope characteristics, we think that the effect will be small due to high ambient relative humidities (>90%) used in the calculations.

675 The results of the calculations outlined above are summarized in Table 2. It is clear that for atmospheric conditions prevailing during rainy period, represented by 2020/02/10 night time convective event, the degree of partial evaporation of raindrops below the cloud base is negligible (reduction of the mean d excess value in the order of 0.1%). This stems mainly from the low elevation of the mean cloud level above the local ground and the resulting short travel time of raindrops to the surface, as well as very high relative humidity of ambient atmosphere below the cloud base. In contrast, the calculations performed for the 24/02/2021 day time event indicate that, for the situations with relatively high elevation of the cloud base level and low ambient relative humidity of the atmosphere beneath this level, the impact of partial evaporation of raindrops on their isotope characteristics can be substantial.

4. Discussion

685 Detailed evaluations of isotopic variability in convective rainfall were provided by both inter- and intra-events. Such separation between inter- and intra-events allows for improved evaluation of fractionation processes that occurred during moisture transport towards the formation of local rainfall. Generally, during the summer, thermal conditions dominate convective processes, while during autumn and spring, convective rainfall is associated with frontal systems (Fig. 2). It is crucial to quantify these synoptic variations to understand seasonal differences in atmospheric conditions, which affect moisture source and transport across seasons. Thus, the δ_{initial} values are influenced by vapor origin, convective activity, and weather systems, which may be further modified by local processes, resulting in distinct values of δ_{med} and large $\Delta\delta$.

690 The key regional and local controls of the isotopic composition of convective rainfall are, respectively: (i) rainfall of moist air masses during their transport in the atmosphere, from the source region(s) to the collection site showed by inter-event analysis, and (ii) local effects associated with convective cloud characteristics, vertical rainfall structure and near-surface humidity conditions.

4.1 Regional atmospheric controls

695 Regional aspects of atmospheric moisture transport to the Rio Claro site were illustrated in HYSPLIT backward trajectories (Fig. 3) and maps of vertically integrated moisture flux in the region (Fig. 4). Most of moist air masses arriving at Rio Claro

700 during summer (2020/02/10, 2020/02/01, and 2020/01/30) exhibited a common origin in the equatorial Atlantic Ocean and were subjected to a long rainfall of moist air masses, extending over several thousand kilometers. Along this pathway, air masses interacted with the Amazon forest. Intensive recycling of moisture leads to a small continental gradient of δ -values of rainfall across the Amazon forest (Salati et al., 1979; Rozanski et al., 1993) and elevated d -excess (Gat, J. R., & Matsui, 1991). At Rio Claro, the arriving air masses are depleted in heavy isotopes ($\delta_{\text{initial}} < -10.0$ ‰) due to enhanced amount of rainfall along the trajectories (> 78 mm), after the southeastern deflection from the Andes, with consistent initial d -excess higher than +10.0 ‰, inherited through the interaction of maritime moisture with the Amazon forest. In contrast, the summer event on 2021/02/24 was influenced by oceanic moisture and had a short trajectory compared to the other summer events, as indicated by the lower amount of rainfall along the Hysplit trajectory (53 mm), which explains the higher δ_{initial} values ($\delta^{18}\text{O} = -7.6$ ‰ and d -excess = +13 ‰).

705 The convective events representing spring and autumn season exhibited substantially shorter trajectories suggesting that the atmospheric “pump” transporting moisture from the equatorial Atlantic Ocean to the Amazon forest was much weaker or non-existent during this time of the year. As a result, those trajectories were characterized by a reduction in the amount of rainfall along the trajectories and enriched δ_{initial} (≥ -3.1 ‰) and higher initial d -excess ($> +10.0$ ‰).

710 In addition, the highest initial d -excess (≥ 24.1 ‰) were observed on 2019/11/05 and 2020/09/06 events. A possible explanation of these greater d -excess values may be enhanced interaction with the surface of the continent, resulting in evapotranspiration processes. At steady state, transpiration is a non-fractionating process. This means that soil water pumped by plants returns to the atmosphere without any detectable change in its isotopic composition (Cuntz et al., 2007; Flanagan et al., 1991; Dongmann and Nürnberg, 1974). If it is assumed that soil water available to plants has isotopic characteristics equal to the mean values of the two events described, then the water vapor released to the local atmosphere during transpiration will possess identical isotopic signatures. Now, assuming that this water vapor is lifted by convection and then condenses, it is possible to easily calculate the isotopic composition of the first condensate. Assuming an isotopic equilibrium between the gaseous and liquid phases of water in the cloud:

$$720 \delta_L = \alpha_{eq}(1000 + \delta_V) - 1000 \quad (7)$$

725 where δ_L and δ_V signify delta values of liquid (condensate) and vapor phase, respectively, at isotopic equilibrium, whereas α_{eq} stands for equilibrium fractionation factor. Equilibrium fractionation factors for ^2H , ^{18}O and d -excess were calculated using empirical expressions proposed by (Horita and Wesolowski, 1994). The assumed condensation temperature was equal 20 °C and 18 °C (cf. Tdw for 2019/11/05 and 2020/06/09, respectively in Table 1). The calculated isotopic characteristics of the first condensate are equal $\delta^2\text{H} = +85.1$ ‰, $\delta^{18}\text{O} = +6.6$ ‰, d -excess = +32.3 ‰ and $\delta^2\text{H} = +81.0$ ‰, $\delta^{18}\text{O} = +6.5$ ‰, d -excess = +28.8 ‰, for both respectively events. This example calculation suggests the transpiration process could generate isotopically enriched rainfall and greater d -excess.

Thus, these regional processes were imprinted in the initial isotopic composition ($\delta^{18}\text{O}_{\text{initial}}$ and d -excess) of all convective events. This regional δ -signature was preserved during summer (2020/01/30 and 2020/02/01), autumn (2020/06/09) and spring

730 (2019/11/05) events, as indicated by similar $\delta^{18}\text{O}_{\text{initial}}$, $\delta^{18}\text{O}_{\text{med}}$, lower $\Delta\delta^{18}\text{O}$ values. In addition, the d -excess exhibited greater
735 difference between δ_{initial} and δ_{med} , and higher $\Delta\delta$ values in relation to the $\delta^{18}\text{O}$ parameters for all convective rainfall events.
The following section provides more detail on the variability of d -excess in terms of local atmospheric processes.

4.2 Local atmospheric controls

The events on summer (2020/02/10 and 2021/02/24), autumn (2020/05/23) and spring (2020/11/18) exhibited substantial
735 differences in δ_{initial} , δ_{med} , and higher $\Delta\delta$ for $\delta^{18}\text{O}$, $\delta^2\text{H}$ and d -excess (Table 1), implying that local processes modified the
regional isotopic imprint.

Overall, the Rayleigh distillation governs the depletion of isotopic composition for the events 2020/02/10 ($^{18}\text{O}_{\text{initial}} = -12.3$
740 ‰ and $\delta^{18}\text{O}_{\text{med}} = -13.9 \text{‰}$) and 2020/11/18 ($^{18}\text{O}_{\text{initial}} = -2.7 \text{‰}$ and $\delta^{18}\text{O}_{\text{med}} = -4.1 \text{‰}$). This depletion is linked to a reduction of
isotopic exchange and the local increase in cloud-top heights, which leads to a rise in BT values observed at both events,
ranging from -16 to -45 °C (Fig. 5I) and -62 and -65 °C (Fig. 6I), respectively. The intra-event analysis facilitates identification
745 of variable fractionation processes during the evolution of these rainfall systems. The $\delta^{18}\text{O}$ trends of both events show
similarities, but notable differences in d -excess trends occur due to varying vertical profiles and RH conditions. On 2020/02/10,
the Zc changed towards the end of the event while RH remained consistently high (97 %). This induced a change in d -excess
during a specific time of the event. On the other hand, on 2020/11/18, Zc was varied at the beginning of event with lower RH
of 70 ~ 82 %, leading to a lower d -excess during the start of event. The observed strong and significant correlations between
isotopic composition and RH support this variation for both events.

The event of 2021/02/24 provides a suitable example of the impact of local factors. The marked differences between the
initial and median values for d -excess (13 ‰ and 7.2 ‰, respectively) and the isotopic composition, enriched with initial
750 ($\delta^{18}\text{O}_{\text{initial}} = -7.6 \text{‰}$ and $\delta^2\text{H}_{\text{initial}} = -47.8 \text{‰}$) and median ($\delta^{18}\text{O}_{\text{med}} = -6.8 \text{‰}$ and $\delta^2\text{H}_{\text{med}} = -44.8 \text{‰}$) values (Table 1), resulted in a
distinctive enrichment in the isotopic composition. This enrichment is associated with the diverse vertical structure of rainfall
and low humidity conditions (RH, 78 ~ 88%). Alterations in both rainfall patterns and Zc levels under low humidity conditions
promote the preferential escape of lighter isotopologues from liquid water (Dansgaard, 1964). This is corroborated by notable
and negative correlations between isotopic composition, rainfall volume, and Zc. In addition, the preferential escape of lighter
isotopologues also occurred during the 2020/05/23, characterized by lower RH (78 ~ 89 %), resulted in enriched isotopic
755 composition.

The semi-quantitative evaluation illustrated in Table 2 reinforces the intra-event analysis, suggesting a modification of the
mean d -excess. The intra-event results indicate that local changes in the isotopic composition of rainfall are controlled by the
specific cloud characteristics and the vertical structure of rainfall, which are connected to local humidity conditions. Therefore,
760 the reduction in d -excess was greater during the events on 2021/02/24, 2020/05/23, and 2020/11/18 due to cloud features and
low humidity conditions, compared to the event on 2020/02/10 that had high local humidity conditions.

4 Concluding remarks

The results of this work provide deeper insights into the mechanisms controlling the isotopic variability of convective rainfall in the inland tropics of Brazil. High frequency sampling of rainfall, covering a 1.5 year period (September 2019 – February 2021), was combined with extensive monitoring of meteorological parameters of the local atmosphere, satellite imagery and HYSPLIT backward trajectory modelling of moist air masses bringing rainfall the Rio Claro site, a continental, tropical location in the south eastern Brazil. In total, 90 samples representing eight convective events covering three seasons (summer, autumn and spring) have been collected and analyzed.

On the monthly time scale, the Rio Claro site reveals typical variability observed in other tropical sites, with high amount of rainfall during the rainy period, strongly depleted in heavy isotopes, and high δ values during the dry period. The high frequency isotope and meteorological data gathered in this study allowed to address the reasons of this strong seasonal variability of isotope characteristics of convective rainfall in some detail. The isotope characteristics of the analysed events representing the rainy period, combined with dedicated Hysplit modelling of moist air masses associated with those events, suggest that overwhelming majority rainfall falling in south eastern Brazil during austral summer is generated by moist air masses originating in the equatorial Atlantic Ocean. They pass the entire Amazon basin from east to west, interacting on the way with the rainforest through intense moisture recycling. Deflected by the Andes, they continue to the southeastern Brazil where they lose their high moisture load. It is hard to overestimate the importance of this regional atmospheric moisture transport scheme for the southeastern Brazil in the context of ongoing deforestation of the Amazon rainforest and progressing climate change. Possible weakening of the extent of moisture recycling over the Amazon rainforest may result in substantial reduction of precipitation amount in southeastern Brazil, with grave consequences for the Brazilian economy.

Peculiar isotope characteristics of the autumn and spring rainfall events analysed in this study, combined with dedicated Hysplit modelling of backward trajectories of moist air masses, strongly suggest that rainfall associated with the dry period in the region, largely originates from moisture of continental origin. This moisture flux is generated in evapotranspiration processes returning water stored in the soil column and in the surface water bodies predominantly during the rainy period. It should be emphasized that isotope characteristics of dry season rainfall provided a decisive argument in this respect.

Finally, thanks to high resolution isotope and meteorological data generated in this study, the impact of purely local processes, such as below cloud partial evaporation of raindrops on the isotopic composition of convective rainfall could be assessed. This semi quantitative assessment confirmed that under specific conditions (high cloud base position in the local atmosphere, moderate or low relative humidity of ambient relative humidity of the atmosphere beneath this level), the impact of partial evaporation of raindrops on their isotope characteristics can be substantial.

Although high frequency rainfall sampling is logistically difficult, we encourage future studies of this type in different geographical regions across the tropics, to better understand the factors controlling the isotopic composition of convective

rainfall during rainy period. Such studies should be accompanied by extensive monitoring of local meteorological parameters and modelling of regional transport of moisture to the rainfall collection site.

795 **5 Concluding remarks**

The study employed high-frequency isotope parameters (δ_{initial} , δ_{med} , and $\Delta\delta$) as well as meteorological data to investigate the regional and local mechanisms controlling the isotopic characteristics of convective precipitation.

800 Based on inter-event analysis, it has been revealed that the regional isotopic characteristics are different between summer and autumn-spring seasons. The δ_{initial} is determined by moisture transport mechanisms and convection features. The key factors are progressive rainfall along trajectories and Rayleigh distillation along the moisture transport pathway. The effect of rainfall along trajectories is pronounced during summer events, associated with the longer moisture transport pathway from the Amazon forest, which produces depleted heavy isotopes. In contrast, reduced autumn and spring rainfall along trajectories are associated with the shorter moisture transport pathway from the Atlantic Ocean and southern Brazil, producing enriched isotope characteristics. This regional δ -signature has been preserved in both summer, autumn, and spring events. Specific events in autumn and spring with high d -excess values were associated with evapotranspiration processes along the moisture transport pathway, demonstrating how regional convective processes interact with the tropical surface and alter the isotopic composition.

805 During the advance of convective rainfall, the regional δ -signature was altered by local effects generated the isotope variability (large $\Delta\delta$ values), as shown by the intra-event evaluation. The critical local controls are the cloud changes and the vertical structure of the rainfall. The local controls occur under certain specific conditions of low relative humidity of ambient. These local mechanisms amplify the discrepancy between the δ_{initial} and δ_{med} values, leading to significant $\Delta\delta$ values. Significant correlations between $\delta^{18}\text{O}$, d -excess, Z_c , and RH, as well as the semi-quantitative evaluation, lend support to the significance of the vertical structure and relative humidity conditions outlined in this study.

810 Therefore, the convective rainfall is controlled by an interplay of regional and local factors. The complex and dynamic conditions of convective rainfall formation across the tropics can be understood using high-frequency analysis. Through identifying the complexity of the factors that make up the isotopic composition of convective rainfall in the study area, it was possible to understand why it was so difficult to apply regression models in past studies when using daily data and separation of rainfall types for the Rio Claro GNIP station.

815 Although high-frequency rainfall sampling is logistically difficult, we encourage future studies of this type in different geographical regions across the tropics, to better understand the factors controlling the isotopic composition of convective rainfall during rainy period. Extensive monitoring of local meteorological parameters and modeling of regional moisture transport to the rainfall collection site, along with the application of more robust below-cloud models, should accompany such studies.

Data availability

825 A complete database (isotope characteristics of rainfall as well as selected meteorological parameters characterizing these
events) are available at: <https://doi.org/10.17632/kk3gs8zn4s.1> (dos Santos et al., 2023). Monthly GNIP data:
<https://www.iaea.org/services/networks/gnip>. GOES-16 imageries are available at:
https://home.chpc.utah.edu/~u0553130/Brian_Blaylock/cgi-bin/goes16_download.cgi. The weather systems are available at:
<https://www.marinha.mil.br/chm/dados-do-smm-cartas-sinoticas/cartas-sinoticas> and
830 <http://tempo.cptec.inpe.br/boletimtecnico/pt>. Reanalysis data are available at:
<https://cds.climate.copernicus.eu/cdsapp#!/search?type=dataset>. The Global Modeling and Assimilation Office (GMAO) data
are available at: <https://goldsmr4.gesdisc.eosdis.nasa.gov/data/MERRA2/M2T1NXFLX.5.12.4/>.
Goddard Earth Sciences Data and Information Services Center (GES DISC) data are available at:
https://disc.gsfc.nasa.gov/datasets/AIRS3STD_7.0/summary.

Formatado: Recuo: Primeira linha: 0 cm

Financial support

This work was funded by grants the São Paulo Research Foundation (FAPESP) under Processes 2018/06666-4, 2019/03467-3 and 2021/10538-4, and by the International Atomic Energy Agency Grant CRP-F31006.

Acknowledgment

840 FAPESP support for the scholarship provided under the Process 2019/03467-3 and 2021/10538-4 is acknowledged. Durán-Quesada acknowledges time for analysis and writing provided within UCR C1038 project. [The authors acknowledge Troy G. for English revision.](#)

References

- 845 Adler, R. F. and Fenn, D. D.: Thunderstorm Vertical Velocities Estimated from Satellite Data, *American*, 36, 1747–1754, [https://doi.org/10.1175/1520-0469\(1979\)036<1747:TVVEFS.2.0.CO;2](https://doi.org/10.1175/1520-0469(1979)036<1747:TVVEFS.2.0.CO;2), 1979.
- Adler, R. F. and Mack, R. A.: Thunderstorm Cloud Top Dynamics as Inferred from Satellite Observations and a Cloud Top Parcel Model, *American Meteorological Society*, 43, 1945–1960, [https://doi.org/10.1175/1520-0469\(1986\)043<1945:TCTDAI.2.0.CO;2](https://doi.org/10.1175/1520-0469(1986)043<1945:TCTDAI.2.0.CO;2), 1986.
- Aemisegger, F., Spiegel, J. K., Pfahl, S., Sodemann, H., Eugster, W., and Wernli, H.: Isotope meteorology of cold front passages: A case study combining observations and modeling, *Geophysical Research Letters*, 42, 5652–5660, <https://doi.org/10.1002/2015GL063988>, 2015.
- Aggarwal, P. K., Romatschke, U., Araguas-Araguas, L., Belachew, D., Longstaffe, F. J., Berg, P., Schumacher, C., and Funk,

- 855 A.: Proportions of convective and stratiform precipitation revealed in water isotope ratios, *Nature Geoscience*, 9, 624–629, <https://doi.org/10.1038/ngeo2739>, 2016.
- Barras, V. and Simmonds, I.: Observation and modeling of stable water isotopes as diagnostics of rainfall dynamics over southeastern Australia, *Journal of Geophysical Research Atmospheres*, 114, <https://doi.org/10.1029/2009JD012132>, 2009.
- Celle-jeanton, H., Gonfiantini, R., Travi, Y., and Sol, B.: Oxygen-18 variations of rainwater during precipitation: Application of the Rayleigh model to selected rainfalls in Southern France, *Journal of Hydrology*, 289, 165–177, <https://doi.org/10.1016/j.jhydrol.2003.11.017>, 2004.
- 860 Coplen, T. B., Neiman, P. J., White, A. B., Landwehr, J. M., Ralph, F. M., and Dettinger, M. D.: Extreme changes in stable hydrogen isotopes and precipitation characteristics in a landfalling Pacific storm, *Geophysical Research Letters*, 35, L21808, <https://doi.org/10.1029/2008GL035481>, 2008.
- 865 Craig, H. and Gordon, L. I.: Deuterium and oxygen-18 variations in the ocean and the marine atmosphere., edited by: Tongiorgi, E., *Stable isotopes in oceanographic and paleotemperatures*, Pisa, 9–130 pp., 1965.
- Cuntz, M., Ogee, J., Farquhar, G. D., Peylin, P., and Cernusak, L. A.: Modelling advection and diffusion of water isotopologues in leaves, *Plant, Cell and Environment*, 30, 892–909, <https://doi.org/10.1111/j.1365-3040.2007.01676.x>, 2007.
- Dansgaard, W.: Stable isotopes in precipitation, *Tellus*, 16, 436–468, <https://doi.org/10.3402/tellusa.v16i4.8993>, 1964.
- 870 Donat, M. G., Alexander, L. V., Yang, H., Durre, I., Vose, R., Dunn, R. J. H., Willett, K. M., Aguilar, E., Brunet, M., Caesar, J., Hewitson, B., Jack, C., Klein Tank, A. M. G., Kruger, A. C., Marengo, J., Peterson, T. C., Renom, M., Oria-Rojas, C., Rusticucci, M., Salinger, J., Elrayah, A. S., Sekele, S. S., Srivastava, A. K., Trewin, B., Villarroya, C., Vincent, L. A., Zhai, P., Zhang, X., and Kitching, S.: Updated analyses of temperature and precipitation extreme indices since the beginning of the twentieth century: The HadEX2 dataset, *Journal of Geophysical Research Atmospheres*, 118, 2098–2118, <https://doi.org/10.1002/jgrd.50150>, 2013.
- 875 Dongmann, G. and Nürnberg, H. W.: On the Enrichment of H²18O in the Leaves of Transpiring Plants, *Radiation and Environmental Biophysics*, 52, 41–52, 1974.
- Endries, J. L., Perry, L. B., Yuter, S. E., Seimon, A., Andrade-Flores, M., Winkelmann, R., Quispe, N., Rado, M., Montoya, N., Velarde, F., and Arias, S.: Radar-observed characteristics of precipitation in the tropical high andes of Southern Peru and Bolivia, *Journal of Applied Meteorology and Climatology*, 57, 1441–1458, <https://doi.org/10.1175/JAMC-D-17-0248.1>, 2018.
- 880 van der Ent, R. J. and Tuinenburg, O. A.: The residence time of water in the atmosphere revisited, *Hydrology and Earth System Sciences*, 21, 779–790, <https://doi.org/10.5194/hess-21-779-2017>, 2017.
- Flanagan, L. B., Comstock, J. P., and Ehleringer, J. R.: Comparison of modeled and observed environmental influences on the stable oxygen and hydrogen isotope composition of leaf water in *Phaseolus vulgaris* L., *Plant Physiology*, 96, 588–596, <https://doi.org/10.1104/pp.96.2.588>, 1991.
- 885 Froehlich, K., Gibson, J. J., and Aggarwal, P.: Deuterium excess in precipitation and its climatological significance, *Journal of Geophysical Research Atmospheres*, 1, 23, 2002.
- Gadgil, S.: The Indian monsoon and its variability, *Annual Review of Earth and Planetary Sciences*, 31, 429–467,

<https://doi.org/10.1146/annurev.earth.31.100901.141251>, 2003.

890 García Santos, S., Sánchez Murillo, R., Peña Paz, T., Chirinos Escobar, M. J., Hernández Ortiz, J. O., Mejía Escobar, E. J.,
and Ortega, L.: Water stable isotopes reveal a complex rainfall to groundwater connectivity in central Honduras, *Science of the
Total Environment*, 844, <https://doi.org/10.1016/j.scitotenv.2022.156941>, 2022.

Garreaud, R. D.: Cold air incursions over subtropical South America: Mean structure and dynamics, *Monthly Weather Review*,
128, 2544–2559, [https://doi.org/10.1175/1520-0493\(2000\)128<2544:caioss>2.0.co;2](https://doi.org/10.1175/1520-0493(2000)128<2544:caioss>2.0.co;2), 2000.

895 Gat, J. R., & Matsui, E.: Atmospheric water balance in the Amazon Basin: An isotopic evapotranspiration model, *Journal of
Geophysical Research*, 96, 13179–13188, <https://doi.org/https://doi.org/10.1029/91JD00054>, 1991.

Gat, J. R.: *Environmental isotopes in the hydrological cycle: Principles and applications. Volume II, Atmospheric water*,
Technical documents in hydrology, Paris, 1–113 pp., 2001.

900 Gedzelman, S. D. and Lawrence, J. R.: The Isotopic Composition of Precipitation from Two Extratropical Cyclones, *American
Meteorological Society*, 118, 495–509, [https://doi.org/10.1175/1520-0493\(1990\)118,0495:TICOPF.2.0.CO;2](https://doi.org/10.1175/1520-0493(1990)118,0495:TICOPF.2.0.CO;2), 1990.

Gimeno, L., Drumond, A., Nieto, R., Trigo, R. M., and Stohl, A.: On the origin of continental precipitation, *Geophysical
Research Letters*, 37, 1–7, <https://doi.org/10.1029/2010GL043712>, 2010.

905 Gimeno, L., Vázquez, M., Eiras Barea, J., Sorí, R., Stojanovic, M., Algarra, I., Nieto, R., Ramos, A. M., Durán Quesada, A.
M., and Dominguez, F.: Recent progress on the sources of continental precipitation as revealed by moisture transport analysis,
Earth Science Reviews, 201, 103070, <https://doi.org/10.1016/j.earscirev.2019.103070>, 2020.

Gonfiantini, R.: Environmental isotopes in lake studies, in: *Handbook of Environmental Isotope Geochemistry Vol. 2 The
Terrestrial Environment*, vol. 2, Elsevier, Amsterdam, 113–168, 1986.

910 Graf, P., Wernli, H., Pfahl, S., and Sodemann, H.: A new interpretative framework for below-cloud effects on stable water
isotopes in vapour and rain, *Atmospheric Chemistry and Physics*, 19, 747–765, <https://doi.org/10.5194/aep-19-747-2019>,
2019.

Han, X., Lang, Y., Wang, T., Liu, C.-Q., Li, F., Wang, F., Guo, Q., Li, S., Liu, M., Wang, Y., and Xu, A.: Temporal and spatial
variations in stable isotopic compositions of precipitation during the typhoon Lekima (2019), China, *Science of The Total
Environment*, 762, 143143, <https://doi.org/10.1016/j.scitotenv.2020.143143>, 2021.

Horita, J. and Wesolowski, D. J.: Horita and Wesolowski 1994, *Geochimica et Cosmochimica Acta*, 58, 1–13, 1994.

915 Horita, J., Rozanski, K., and Cohen, S.: Isotope effects in the evaporation of water: a status report of the Craig–Gordon model,
Isotopes in Environmental and Health Studies, 44, 23–49, <https://doi.org/10.1080/10256010801887174>, 2008.

Houze, R.: Stratiform precipitation in regions of convection: A Meteorological Paradox?, *Bulletin of the American
Meteorological Society*, 78, 2179–2195, 1997.

Houze, R. A.: *Cloud dynamics*, Academic Press Limited, 573 pp., [https://doi.org/10.1016/0377-0265\(87\)90017-0](https://doi.org/10.1016/0377-0265(87)90017-0), 1993.

920 Houze, R. A.: Mesoscale Convective Systems, in: *International Geophysics*, vol. 104, 237–286, <https://doi.org/10.1016/B978-0-12-374266-7.00009-3>, 2004.

Houze, R. A. J.: Observed structure of mesoscale convective systems and implications for large-scale heating., *Quart. J. Roy.*

- Meteor. Soc., 115, 425–461, 1989.
- 925 Hu, J., Emile-Geay, J., Nusbaumer, J., and Noone, D.: Impact of Convective Activity on Precipitation $\delta^{18}\text{O}$ in Isotope-Enabled General Circulation Models, *Journal of Geophysical Research: Atmospheres*, 123, 13,595–13,610, <https://doi.org/10.1029/2018JD029187>, 2018.
- IAEA: IAEA / GNIP precipitation sampling guide V2.02, Global Network of Isotopes in Precipitation (GNIP), 20, 2014.
- IPCC, W. G. I. T. P. S. B.: Regional fact sheet—Central and South America, Sixth Assessment Report, 1–2 pp., 2021.
- 930 Jeelani, G., Deshpande, R. D., Galkowski, M., and Rozanski, K.: Isotopic composition of daily precipitation along the southern foothills of the Himalayas: Impact of marine and continental sources of atmospheric moisture, *Atmospheric Chemistry and Physics*, 18, 8789–8805, <https://doi.org/10.5194/acp-18-8789-2018>, 2018.
- Klaassen, W.: Radar Observations and Simulation of the Melting Layer of Precipitation, *Journal of the Atmospheric Sciences*, 45, 3741–3753, 1988.
- 935 Kodama, Y.: Large-scale common features of subtropical precipitation zones (the Baiu Frontal Zone, the SPCZ, and the SACZ) Part I: Characteristics of subtropical frontal zones, *Journal of the Meteorological Society of Japan*, 70, 813–836, <https://doi.org/10.1248/epb.37.3229>, 1992.
- Kurita, N.: Water isotopic variability in response to mesoscale convective system over the tropical ocean, *Journal of Geophysical Research Atmospheres*, 118, 10,376–10,390, <https://doi.org/10.1002/jgrd.50754>, 2013.
- 940 Lawrence, J. R., Gedzelman, S. D., Dexheimer, D., Cho, H. K., Carrie, G. D., Gasparini, R., Anderson, C. R., Bowman, K. P., and Biggerstaff, M. I.: Stable isotopic composition of water vapor in the tropics, *Journal of Geophysical Research Atmospheres*, 109, 16, <https://doi.org/10.1029/2003jd004046>, 2004.
- Lee, J. and Fung, I.: “Amount effect” of water isotopes and quantitative analysis of post-condensation processes, *Hydrological Processes*, 22, 1–8, <https://doi.org/10.1002/hyp.6637>, 2008.
- 945 Lekshmy, P. R., Midhun, M., Ramesh, R., and Jani, R. A.: ^{18}O depletion in monsoon rain relates to large-scale organized convection rather than the amount of rainfall, *Scientific Reports*, 4, 1–5, <https://doi.org/10.1038/srep05661>, 2014.
- Luiz Silva, W., Xavier, L. N. R., Maceira, M. E. P., and Rotunno, O. C.: Climatological and hydrological patterns and verified trends in precipitation and streamflow in the basins of Brazilian hydroelectric plants, *Theoretical and Applied Climatology*, 137, 353–371, <https://doi.org/10.1007/s00704-018-2600-8>, 2019.
- 950 Machado, L. A. T. and Rossow, W. B.: Structural Characteristics and Radiative Properties of Tropical Cloud Clusters, *Monthly Weather Review*, 121, 3234–3260, 1993.
- Machado, L. A. T., Rossow, W. B., Guedes, R. L., and Walker, A. W.: Life cycle variations of mesoscale convective systems over the Americas, *Monthly Weather Review*, 126, 1630–1654, [https://doi.org/10.1175/1520-0493\(1998\)126<1630:LCVOMC>2.0.CO;2](https://doi.org/10.1175/1520-0493(1998)126<1630:LCVOMC>2.0.CO;2), 1998.
- 955 Marengo, J. A., Soares, W. R., Saulo, C., and Nicolini, M.: Climatology of the low-level jet east of the Andes as derived from the NCEP-NCAR reanalyses: Characteristics and temporal variability, *Journal of Climate*, 17, 2261–2280, [https://doi.org/10.1175/1520-0442\(2004\)017<2261:COTLJE>2.0.CO;2](https://doi.org/10.1175/1520-0442(2004)017<2261:COTLJE>2.0.CO;2), 2004.

- Marengo, J. A., Ambrizzi, T., Alves, L. M., Barreto, N. J. C., Simões Reboita, M., and Ramos, A. M.: Changing Trends in Rainfall Extremes in the Metropolitan Area of São Paulo: Causes and Impacts, *Frontiers in Climate*, 2, 1–13, <https://doi.org/10.3389/felim.2020.00003>, 2020.
- 960 Mehta, S., Mehta, S. K., Singh, S., Mitra, A., Ghosh, S. K., and Raha, S.: Characteristics of the Z–R Relationships Observed Using Micro Rain Radar (MRR-2) over Darjeeling (27.05° N, 88.26° E): A Complex Terrain Region in the Eastern Himalayas, *Pure and Applied Geophysics*, 177, 4521–4534, <https://doi.org/10.1007/s00024-020-02472-6>, 2020.
- Moerman, J. W., Cobb, K. M., Adkins, J. F., Sodemann, H., Clark, B., and Tuen, A. A.: Diurnal to interannual rainfall $\delta^{18}\text{O}$ variations in northern Borneo driven by regional hydrology, *Earth and Planetary Science Letters*, 369–370, 108–119, <https://doi.org/10.1016/j.epsl.2013.03.014>, 2013.
- 965 Muller, C. L., Baker, A., Fairchild, I. J., Kidd, C., and Boomer, I.: Intra-Event Trends in Stable Isotopes: Exploring Midlatitude Precipitation Using a Vertically Pointing Micro Rain Radar, *Journal of Hydrometeorology*, 16, 194–213, <https://doi.org/10.1175/JHM-D-14-0038.1>, 2015.
- Munksgaard, N. C., Zwart, C., Haig, J., Cernusak, L. A., and Bird, M. I.: Coupled rainfall and water vapour stable isotope time series reveal tropical atmospheric processes on multiple timescales, *Hydrological Processes*, 34, 111–124, <https://doi.org/10.1002/hyp.13576>, 2020.
- 970 Rao, N. T., Kirankumar, N. V. P., Radhakrishna, B., and Rao, N. D.: Classification of tropical precipitating systems using wind profiler spectral moments. Part I: Algorithm description and validation, *Journal of Atmospheric and Oceanic Technology*, 25, 884–897, <https://doi.org/10.1175/2007JTECHA1031.1>, 2008.
- 975 Ribeiro, B. Z., Machado, L. A. T., Biscaro, T. S., Freitas, E. D., Mozer, K. W., and Goodman, S. J.: An evaluation of the GOES-16 rapid scan for nowcasting in southeastern Brazil: Analysis of a severe hailstorm case, *Weather and Forecasting*, 34, 1829–1848, <https://doi.org/10.1175/WAF-D-19-0070.1>, 2019.
- Risi, C., Bony, S., Vimeux, F., Chong, M., and Deser, L.: Evolution of the stable water isotopic composition of the rain sampled along Sahelian squall lines, *Quarterly Journal of the Royal Meteorological Society*, 136, 227–242, <https://doi.org/10.1002/qj.485>, 2010.
- 980 Roberts, R. D. and Rutledge, S.: Nowcasting storm initiation and growth using GOES-8 and WSR-88D data, *Weather and Forecasting*, 18, 562–584, [https://doi.org/10.1175/1520-0434\(2003\)018<0562:NSIAGU>2.0.CO;2](https://doi.org/10.1175/1520-0434(2003)018<0562:NSIAGU>2.0.CO;2), 2003.
- Romatschke, U. and Houze, R. A.: Extreme summer convection in South America, *Journal of Climate*, 23, 3761–3791, <https://doi.org/10.1175/2010JCLI3465.1>, 2010.
- 985 Romatschke, U. and Houze, R. A.: Characteristics of precipitating convective systems accounting for the summer rainfall of tropical and subtropical South America, *Journal of Hydrometeorology*, 14, 25–46, <https://doi.org/10.1175/JHM-D-12-060.1>, 2013.
- Rozanski, K., Sonntag, C., and Munnich, K. O.: Factors controlling stable isotope composition of European precipitation, *Tellus*, 34, 142–150, <https://doi.org/10.3402/tellusa.v34i2.10796>, 1982.
- 990 Rozanski, K., Araguás-Araguás, L., and Gonfiantini, R.: Isotopic Patterns in Modern Global Precipitation, 1–36,

<https://doi.org/10.1029/GM078p0001>, 1993.

Rezanski, K., Mook, W. G., and Froehlich, K.: *Environmental Isotopes in the Hydrological Cycle: Principles and Applications*, Technical documents in hydrology, Paris, 1–117 pp., 2001.

995 Salati, E., Dall'Olio, A., Matsui, E., and Gat, J. R.: Recycling of water in the Amazon Basin: An isotopic study, *Water Resources Research*, 15, 1250–1258, <https://doi.org/10.1029/WR015i005p01250>, 1979.

Sánchez-Murillo, R., Durán-Quesada, A. M., Birkel, C., Esquivel-Hernández, G., and Boll, J.: Tropical precipitation anomalies and d excess evolution during El Niño 2014–16, *Hydrological Processes*, 31, 956–967, <https://doi.org/10.1002/hyp.11088>, 2017.

1000 Sánchez-Murillo, R., Durán-Quesada, A. M., Esquivel-Hernández, G., Rojas-Cantillano, D., Birkel, C., Welsh, K., Sánchez-Llull, M., Alonso-Hernández, C. M., Tetzlaff, D., Soulsby, C., Boll, J., Kurita, N., and Cobb, K. M.: Deciphering key processes controlling rainfall isotopic variability during extreme tropical cyclones, *Nature Communications*, 10, 1–10, <https://doi.org/10.1038/s41467-019-12062-3>, 2019.

1005 dos Santos, V., Marshall-Fleming, P., Henrique Mancini, L., Dalva Santos-Cota, S., de Lima, G. B., Rodrigues-Gomes, R., Kirchheim, R. E., Sánchez-Murillo, R., and Gastmans, D.: Distinguishing the Regional Atmospheric Controls on Precipitation Isotopic Variability in the Central-Southeast Portion of Brazil, *Advances in Atmospheric Sciences*, 39, 1693–1708, <https://doi.org/10.1007/s00376-022-1367-0>, 2022.

dos Santos, V., Gastmans, D., and Sánchez-Murillo, R.: Isotope and meteorologic database of high-frequency sampling of convective rainfall events in Rio Claro, Brazil, <https://doi.org/10.17632/4kk3gs8zn4s.1>, 2023.

1010 Schmit, T. J., Griffith, P., Gunshor, M. M., Daniels, J. M., Goodman, S. J., and Lebar, W. J.: A closer look at the ABI on the goes-r series, *Bulletin of the American Meteorological Society*, 98, 681–698, <https://doi.org/10.1175/BAMS-D-15-00230.1>, 2017.

Schumacher, C. and Houze, R. A.: Stratiform rain in the tropics as seen by the TRMM precipitation radar, *Journal of Climate*, 16, 1739–1756, [https://doi.org/10.1175/1520-0442\(2003\)016<1739:SRITTA>2.0.CO;2](https://doi.org/10.1175/1520-0442(2003)016<1739:SRITTA>2.0.CO;2), 2003.

1015 Siqueira, J. R., Rossow, W. B., Machado, L. A. T., and Pearl, C.: Structural characteristics of convective systems over South America related to cold frontal incursions, *Monthly Weather Review*, 133, 1045–1064, <https://doi.org/10.1175/MWR2888.1>, 2005.

Sodemann, H.: *Tropospheric transport of water vapour: Lagrangian and Eulerian perspectives*, Swiss Federal Institute of Technology Zurich, 230 pp., 2006.

1020 Soderberg, K., Good, S. P., O'connor, M., Wang, L., Ryan, K., and Caylor, K. K.: Using atmospheric trajectories to model the isotopic composition of rainfall in central Kenya, *Ecosphere*, 4, 1–18, <https://doi.org/10.1890/ES12-00160.1>, 2013.

Stein, A. F., Draxler, R. R., Rolph, G. D., Stunder, B. J. B., Cohen, M. D., and Ngan, F.: NOAA's hysplit atmospheric transport and dispersion modeling system, *Bulletin of the American Meteorological Society*, 96, 2059–2077, <https://doi.org/10.1175/BAMS-D-14-00110.1>, 2015.

Steiner, M. and Smith, J. A.: Convective versus stratiform rainfall: An ice-microphysical and kinematic conceptual model,

1025 Atmospheric Research, 47–48, 317–326, [https://doi.org/10.1016/S0169-8095\(97\)00086-0](https://doi.org/10.1016/S0169-8095(97)00086-0), 1998.

Stewart, M. K.: Stable isotope fractionation due to evaporation and isotopic exchange of falling waterdrops: Applications to atmospheric processes and evaporation of lakes, *Journal of Geophysical Research*, 80, 1133–1146, <https://doi.org/10.1029/JC080i009p01133>, 1975.

Sun, C., Shanahan, T. M., and Partin, J.: Controls on the Isotopic Composition of Precipitation in the South-Central United States, *Journal of Geophysical Research: Atmospheres*, 124, 8320–8335, <https://doi.org/10.1029/2018JD029306>, 2019.

1030 Sun, C., Tian, L., Shanahan, T. M., Partin, J. W., Gao, Y., Piatrunia, N., and Banner, J.: Isotopic variability in tropical cyclone precipitation is controlled by Rayleigh distillation and cloud microphysics, *Communications Earth & Environment*, 3, <https://doi.org/10.1038/s43247-022-00381-1>, 2022.

Taupin, J. D., Gallaire, R., and Arnaud, Y.: Analyses isotopiques et chimiques des précipitations sahélienne de la région de Niamey au Niger: implications climatologiques, *Hydrochemistry*, 151–162, 1997.

1035 Tharammal, T., G. Bala, and D. N.: Impact of deep convection on the isotopic amount effect in tropical precipitation, *Journal of Geophysical Research: Atmospheres*, 122, 1505–1523, <https://doi.org/10.1002/2016JD025555>, 2017.

Tremoy, G., Vimeux, F., Soumana, S., Souley, I., Risi, C., Favreau, G., and Oi, M.: Clustering mesoscale convective systems with laser-based water vapor $\delta^{18}\text{O}$ monitoring in Niamey (Niger), *Journal of Geophysical Research: Atmospheres*, 119, 5079–5103, <https://doi.org/10.1002/2013JD020968>, 2014.

1040 Vila, D. A., Machado, L. A. T., Laurent, H., and Velasco, L.: Forecast and tracking the evolution of cloud clusters (ForTraCC) using satellite infrared imagery: Methodology and validation, *Weather and Forecasting*, 23, 233–245, <https://doi.org/10.1175/2007WAF2006121.1>, 2008.

Vuille, M., Bradley, R. S., Werner, M., Healy, R., and Keimig, F.: Modeling $\delta^{18}\text{O}$ in precipitation over the tropical Americas: 1. Interannual variability and climatic controls, *Journal of Geophysical Research: Atmospheres*, 108, 1–24, <https://doi.org/10.1029/2001JD002038>, 2003.

1045 Wang, T. and Tang, G.: Spatial Variability and Linkage Between Extreme Convections and Extreme Precipitation Revealed by 22-Year Space-Borne Precipitation Radar Data, *Geophysical Research Letters*, 47, 1–10, <https://doi.org/10.1029/2020GL088437>, 2020.

1050 Winnick, M. J., Chamberlain, C. P., Caves, J. K., and Welker, J. M.: Quantifying the isotopic “continental effect,” *Earth and Planetary Science Letters*, 406, 123–133, <https://doi.org/10.1016/j.epsl.2014.09.005>, 2014.

Worden, J., Noone, D., Bowman, K., Beer, R., Eldering, A., Fisher, B., Gunson, M., Goldman, A., Herman, R., Kulawik, S. S., Lampel, M., Osterman, G., Rinsland, C., Rodgers, C., Sander, S., Shephard, M., Webster, C. R., and Worden, H.: Importance of rain evaporation and continental convection in the tropical water cycle, *Nature*, 445, 528–532, <https://doi.org/10.1038/nature05508>, 2007.

1055 World Meteorological Organization: WMO Atlas of Mortality and Economic Losses From Weather, Climate and Water Extremes (1970–2019), Geneva 2, Switzerland, 90 pp., 2021.

Zilli, M. T., Carvalho, L. M. V., Liebmann, B., and Silva Dias, M. A.: A comprehensive analysis of trends in extreme

Formatado: Francês (França)

1060 [precipitation over southeastern coast of Brazil, International Journal of Climatology, 37, 2269–2279, https://doi.org/10.1002/joc.4840, 2017.](https://doi.org/10.1002/joc.4840)

Zwart, C., Munksgaard, N. C., Lambrinidis, D., Bird, M. I., Protat, A., and Kurita, N.: The isotopic signature of monsoon conditions, cloud modes, and rainfall type, *Hydrological Processes*, 2296–2303, <https://doi.org/10.1002/hyp.13140>, 2018.

1065 [Adler, R. F. and Fenn, D. D.: Thunderstorm vertical velocities estimated from satellite data, American, 36, 1747–1754, https://doi.org/10.1175/1520-0469\(1979\)036<1747:TVVEFS.2.0.CO;2, 1979.](https://doi.org/10.1175/1520-0469(1979)036<1747:TVVEFS.2.0.CO;2)

[Adler, R. F. and Mack, R. A.: Thunderstorm cloud top dynamics as inferred from satellite observations and a cloud top parcel model, American Meteorological Society, 43, 1945–1960, https://doi.org/10.1175/1520-0469\(1986\)043.1945:TCTDAI.2.0.CO;2, 1986.](https://doi.org/10.1175/1520-0469(1986)043.1945:TCTDAI.2.0.CO;2)

1070 [Aemisegger, F., Spiegel, J. K., Pfahl, S., Sodemann, H., Eugster, W., and Wernli, H.: Isotope meteorology of cold front passages: A case study combining observations and modeling, Geophysical Research Letters, 42, 5652–5660, https://doi.org/10.1002/2015GL063988, 2015.](https://doi.org/10.1002/2015GL063988)

[Aggarwal, P. K., Romatschke, U., Araguas-Araguas, L., Belachew, D., Longstaffe, F. J., Berg, P., Schumacher, C., and Funk, A.: Proportions of convective and stratiform precipitation revealed in water isotope ratios, Nature Geoscience, 9, 624–629, https://doi.org/10.1038/ngeo2739, 2016.](https://doi.org/10.1038/ngeo2739)

1075 [Bony, S., Risi, C., and Vimeux, F.: Influence of convective processes on the isotopic composition \(\$\delta^{18}\text{O}\$ and \$\delta\text{D}\$ \) of precipitation and water vapor in the tropics: I. Radiative-convective equilibrium and Tropical Ocean–Global Atmosphere–Coupled Ocean–Atmosphere Response Experiment \(TOGA-CO\), Journal of Geophysical Research: Atmospheres, 113, 1–21, https://doi.org/10.1029/2008JD009942, 2008.](https://doi.org/10.1029/2008JD009942)

1080 [Breugem, A. J., Wesseling, J. G., Oostindie, K., and Ritsema, C. J.: Meteorological aspects of heavy precipitation in relation to floods – An overview, Earth-Science Reviews, 204, 103171, https://doi.org/10.1016/j.earscirev.2020.103171, 2020.](https://doi.org/10.1016/j.earscirev.2020.103171)

[Cecchini, M. A., Machado, L. A. T., and Artaxo, P.: Droplet Size Distributions as a function of rainy system type and Cloud Condensation Nuclei concentrations, Atmospheric Research, 143, 301–312, https://doi.org/10.1016/j.atmosres.2014.02.022, 2014.](https://doi.org/10.1016/j.atmosres.2014.02.022)

1085 [Celle-Jeanton, H., Gonfiantini, R., Travi, Y., and Sol, B.: Oxygen-18 variations of rainwater during precipitation: Application of the Rayleigh model to selected rainfalls in Southern France, Journal of Hydrology, 289, 165–177, https://doi.org/10.1016/j.jhydrol.2003.11.017, 2004.](https://doi.org/10.1016/j.jhydrol.2003.11.017)

[Coplen, T. B., Neiman, P. J., White, A. B., Landwehr, J. M., Ralph, F. M., and Dettinger, M. D.: Extreme changes in stable hydrogen isotopes and precipitation characteristics in a landfalling Pacific storm, Geophysical Research Letters, 35, L21808, https://doi.org/10.1029/2008GL035481, 2008.](https://doi.org/10.1029/2008GL035481)

1090 [Craig, H. and Gordon, L. I.: Deuterium and oxygen-18 variations in the ocean and the marine atmosphere., edited by: Tongiorgi, E., Stable isotopes in oceanographic and paleotemperatures, Pisa, 9–130 pp., 1965.](#)

[Cuntz, M., Ogé, J., Farquhar, G. D., Peylin, P., and Cernusak, L. A.: Modelling advection and diffusion of water isotopologues](#)

in leaves, *Plant, Cell and Environment*, 30, 892–909, <https://doi.org/10.1111/j.1365-3040.2007.01676.x>, 2007.

Dansgaard, W.: Stable isotopes in precipitation, *Tellus*, 16, 436–468, <https://doi.org/10.3402/tellusa.v16i4.8993>, 1964.

1095 Donat, M. G., Alexander, L. V., Yang, H., Durre, I., Vose, R., Dunn, R. J. H., Willett, K. M., Aguilar, E., Brunet, M., Caesar, J., Hewitson, B., Jack, C., Klein Tank, A. M. G., Kruger, A. C., Marengo, J., Peterson, T. C., Renom, M., Oria Rojas, C., Rusticucci, M., Salinger, J., Elrayah, A. S., Sekele, S. S., Srivastava, A. K., Trewin, B., Villarreal, C., Vincent, L. A., Zhai, P., Zhang, X., and Kitching, S.: Updated analyses of temperature and precipitation extreme indices since the beginning of the twentieth century: The HadEX2 dataset, *Journal of Geophysical Research Atmospheres*, 118, 2098–2118, <https://doi.org/10.1002/jgrd.50150>, 2013.

1100 Dongmann, G. and Nürnberg, H. W.: On the Enrichment of H218O in the Leaves of Transpiring Plants, *Radiation and Environmental Biophysics*, 52, 41–52, 1974.

Endries, J. L., Perry, L. B., Yuter, S. E., Seimon, A., Andrade-Flores, M., Winkelmann, R., Quispe, N., Rado, M., Montoya, N., Velarde, F., and Arias, S.: Radar-observed characteristics of precipitation in the tropical high andes of Southern Peru and Bolivia, *Journal of Applied Meteorology and Climatology*, 57, 1441–1458, <https://doi.org/10.1175/JAMC-D-17-0248.1>, 2018.

1105 van der Ent, R. J. and Tuinenburg, O. A.: The residence time of water in the atmosphere revisited, *Hydrology and Earth System Sciences*, 21, 779–790, <https://doi.org/10.5194/hess-21-779-2017>, 2017.

Flanagan, L. B., Comstock, J. P., and Ehleringer, J. R.: Comparison of modeled and observed environmental influences on the stable oxygen and hydrogen isotope composition of leaf water in *Phaseolus vulgaris* L, *Plant Physiology*, 96, 588–596, <https://doi.org/10.1104/pp.96.2.588>, 1991.

1110 Froehlich, K., Gibson, J. J., and Aggarwal, P.: Deuterium excess in precipitation and its climatological significance, *Journal of Geophysical Research-Atmospheres*, 1–23, 2002.

Gadgil, S.: The Indian monsoon and its variability, *Annual Review of Earth and Planetary Sciences*, 31, 429–467, <https://doi.org/10.1146/annurev.earth.31.100901.141251>, 2003.

1115 Galewsky, J., Schneider, M., Diekmann, C., Semie, A., Bony, S., Risi, C., Emanuel, K., and Brogniez, H.: The Influence of Convective Aggregation on the Stable Isotopic Composition of Water Vapor, *AGU Advances*, 4, 1–16, <https://doi.org/10.1029/2023AV000877>, 2023.

García-Santos, S., Sánchez-Murillo, R., Peña-Paz, T., Chirinos-Escobar, M. J., Hernández-Ortiz, J. O., Mejía-Escobar, E. J., and Ortega, L.: Water stable isotopes reveal a complex rainfall to groundwater connectivity in central Honduras, *Science of the Total Environment*, 844, <https://doi.org/10.1016/j.scitotenv.2022.156941>, 2022.

1120 Garreaud, R. D.: Cold air incursions over subtropical South America: Mean structure and dynamics, *Monthly Weather Review*, 128, 2544–2559, [https://doi.org/10.1175/1520-0493\(2000\)128<2544:caioss>2.0.co;2](https://doi.org/10.1175/1520-0493(2000)128<2544:caioss>2.0.co;2), 2000.

Gat, J. R., & Matsui, E.: Atmospheric water balance in the Amazon Basin: An isotopic evapotranspiration model, *Journal of Geophysical Research*, 96, 13179–13188, <https://doi.org/https://doi.org/10.1029/91JD00054>, 1991.

1125 Gat, J. R.: Environmental isotopes in the hydrological cycle: Principles and applications. Volume II, Atmospheric water, *Technical documents in hydrology*, Paris, 1–113 pp., 2001.

Gimeno, L., Drumond, A., Nieto, R., Trigo, R. M., and Stohl, A.: On the origin of continental precipitation, *Geophysical Research Letters*, 37, 1–7, <https://doi.org/10.1029/2010GL043712>, 2010.

Gimeno, L., Vázquez, M., Eiras-Barca, J., Sorí, R., Stojanovic, M., Algarra, I., Nieto, R., Ramos, A. M., Durán-Quesada, A. M., and Dominguez, F.: Recent progress on the sources of continental precipitation as revealed by moisture transport analysis, *Earth-Science Reviews*, 201, 103070, <https://doi.org/10.1016/j.earscirev.2019.103070>, 2020.

Gonfiantini, R.: Environmental isotopes in lake studies, in: *Handbook of Environmental Isotope Geochemistry Vol. 2 The Terrestrial Environment*, vol. 2, Elsevier, Amsterdam, 113–168, 1986.

Graf, P., Wernli, H., Pfahl, S., and Sodemann, H.: A new interpretative framework for below-cloud effects on stable water isotopes in vapour and rain, *Atmospheric Chemistry and Physics*, 19, 747–765, <https://doi.org/10.5194/acp-19-747-2019>, 2019.

Han, X., Lang, Y., Wang, T., Liu, C.-Q., Li, F., Wang, F., Guo, Q., Li, S., Liu, M., Wang, Y., and Xu, A.: Temporal and spatial variations in stable isotopic compositions of precipitation during the typhoon Lekima (2019), China, *Science of The Total Environment*, 762, 143143, <https://doi.org/10.1016/j.scitotenv.2020.143143>, 2021.

He, S., Goodkin, N. F., Kurita, N., Wang, X., and Rubin, C. M.: Stable isotopes of Precipitation During Tropical Sumatra Squalls in Singapore, *Journal of Geophysical Research: Atmospheres*, 123, 3812–3829, <https://doi.org/10.1002/2017JD027829>, 2018.

Horita, J. and Wesolowski, D. J.: Horita and Wesolowski 1994, *Geochimica et Cosmochimica Acta*, 58, 1–13, 1994.

Horita, J., Rozanski, K., and Cohen, S.: Isotope effects in the evaporation of water: a status report of the Craig–Gordon model, *Isotopes in Environmental and Health Studies*, 44, 23–49, <https://doi.org/10.1080/10256010801887174>, 2008.

Houze, R.: Stratiform precipitation in regions of convection: A Meteorological Paradox?, *Bulletin of the American Meteorological Society*, 78, 2179–2195, 1997.

Houze, R. A.: *Cloud dynamics*, Academic Press Limited, 573 pp., [https://doi.org/10.1016/0377-0265\(87\)90017-0](https://doi.org/10.1016/0377-0265(87)90017-0), 1993.

Houze, R. A.: Mesoscale Convective Systems, in: *International Geophysics*, vol. 104, 237–286, <https://doi.org/10.1016/B978-0-12-374266-7.00009-3>, 2004.

Houze, R. A. J.: Observed structure of mesoscale convective systems and implications for large-scale heating., *Quart. J. Roy. Meteor. Soc.*, 115, 425–461, 1989.

IAEA: IAEA / GNIP precipitation sampling guide V2.02, *Global Network of Isotopes in Precipitation (GNIP)*, 20, 2014.

IPCC, W. G. I.-T. P. S. B.: Regional fact sheet – Central and South America, *Sixth Assessment Report*, 1–2 pp., 2021.

Jeelani, G., Deshpande, R. D., Galkowski, M., and Rozanski, K.: Isotopic composition of daily precipitation along the southern foothills of the Himalayas: Impact of marine and continental sources of atmospheric moisture, *Atmospheric Chemistry and Physics*, 18, 8789–8805, <https://doi.org/10.5194/acp-18-8789-2018>, 2018.

Kastman, J., Market, P., Fox, N., Foscatto, A., and Lupo, A.: Lightning and Rainfall Characteristics in Elevated vs. Surface Based Convection in the Midwest that Produce Heavy Rainfall, *Atmosphere*, 8, 36, <https://doi.org/10.3390/atmos8020036>, 2017.

Klaassen, W.: Radar Observations and Simulation of the Melting Layer of Precipitation, *Journal of the Atmospheric Sciences*, 45, 3741–3753, 1988.

Kodama, Y.: Large-scale common features of subtropical precipitation zones (the Baiu Frontal Zone , the SPCZ , and the SACZ) Part I: Characteristics of subtropical frontal zones, *Journal of the Meteorological Society of Japan*, 70, 813–836,

1165 <https://doi.org/10.1248/cpb.37.3229>, 1992.

Kurita, N.: Water isotopic variability in response to mesoscale convective system over the tropical ocean, *Journal of Geophysical Research Atmospheres*, 118, 10376–10390, <https://doi.org/10.1002/jgrd.50754>, 2013.

Kurita, N., Ichiyangi, K., Matsumoto, J., Yamanaka, M. D., and Ohata, T.: The relationship between the isotopic content of precipitation and the precipitation amount in tropical regions, *Journal of Geochemical Exploration*, 102, 113–122, 1170 <https://doi.org/10.1016/j.gexplo.2009.03.002>, 2009.

Lacour, J. L., Risi, C., Worden, J., Clerbaux, C., and Coheur, P. F.: Importance of depth and intensity of convection on the isotopic composition of water vapor as seen from IASI and TES δD observations, *Earth and Planetary Science Letters*, 481, 387–394, <https://doi.org/10.1016/j.epsl.2017.10.048>, 2018.

Lawrence, J. R., Gedzelman, S. D., Dexheimer, D., Cho, H., Carrie, G. D., Gasparini, R., Anderson, C. R., Bowman, K. P., 1175 and Biggerstaff, M. I.: Stable isotopic composition of water vapor in the tropics, *Journal of Geophysical Research: Atmospheres*, 109, 16, <https://doi.org/10.1029/2003JD004046>, 2004.

Lee, J. and Fung, I.: “Amount effect” of water isotopes and quantitative analysis of post-condensation processes, *Hydrological Processes*, 22, 1–8, <https://doi.org/10.1002/hyp.6637>, 2008.

Lekshmy, P. R., Midhun, M., Ramesh, R., and Jani, R. A.: ^{18}O depletion in monsoon rain relates to large scale organized 1180 convection rather than the amount of rainfall, *Scientific Reports*, 4, 1–5, <https://doi.org/10.1038/srep05661>, 2014.

Lima, K. C., Satyamurty, P., and Fernández, J. P. R.: Large-scale atmospheric conditions associated with heavy rainfall episodes in Southeast Brazil, *Theoretical and Applied Climatology*, 101, 121–135, <https://doi.org/10.1007/s00704-009-0207-9>, 2010.

Luiz Silva, W., Xavier, L. N. R., Maceira, M. E. P., and Rotunno, O. C.: Climatological and hydrological patterns and verified 1185 trends in precipitation and streamflow in the basins of Brazilian hydroelectric plants, *Theoretical and Applied Climatology*, 137, 353–371, <https://doi.org/10.1007/s00704-018-2600-8>, 2019.

Machado, L. A. T. and Rossow, W. B.: Structural Characteristics and Radiative Properties of Tropical Cloud Clusters, *Monthly Weather Review*, 121, 3234–3260, 1993.

Machado, L. A. T., Rossow, W. B., Guedes, R. L., and Walker, A. W.: Life cycle variations of mesoscale convective systems 1190 over the Americas, *Monthly Weather Review*, 126, 1630–1654, [https://doi.org/10.1175/1520-0493\(1998\)126<1630:LCVOMC>2.0.CO;2](https://doi.org/10.1175/1520-0493(1998)126<1630:LCVOMC>2.0.CO;2), 1998.

Marengo, J. A., Soares, W. R., Saulo, C., and Nicolini, M.: Climatology of the low-level jet east of the Andes as derived from the NCEP-NCAR reanalyses: Characteristics and temporal variability, *Journal of Climate*, 17, 2261–2280, [https://doi.org/10.1175/1520-0442\(2004\)017<2261:COTLJE>2.0.CO;2](https://doi.org/10.1175/1520-0442(2004)017<2261:COTLJE>2.0.CO;2), 2004.

- 1195 [Marengo, J. A., Ambrizzi, T., Alves, L. M., Barreto, N. J. C., Simões Reboita, M., and Ramos, A. M.: Changing Trends in Rainfall Extremes in the Metropolitan Area of São Paulo: Causes and Impacts, *Frontiers in Climate*, 2, 1–13, <https://doi.org/10.3389/fclim.2020.00003>, 2020.](#)
- [Marengo, J. A., Camarinha, P. I., Alves, L. M., Diniz, F., and Betts, R. A.: Extreme Rainfall and Hydro-Geo-Meteorological Disaster Risk in 1.5, 2.0, and 4.0°C Global Warming Scenarios: An Analysis for Brazil, *Frontiers in Climate*, 3, 1–17, <https://doi.org/10.3389/fclim.2021.610433>, 2021.](#)
- 1200 [Mehta, S., Mehta, S. K., Singh, S., Mitra, A., Ghosh, S. K., and Raha, S.: Characteristics of the Z–R Relationships Observed Using Micro Rain Radar \(MRR-2\) over Darjeeling \(27.05° N, 88.26° E\): A Complex Terrain Region in the Eastern Himalayas, *Pure and Applied Geophysics*, 177, 4521–4534, <https://doi.org/10.1007/s00024-020-02472-6>, 2020.](#)
- [Moerman, J. W., Cobb, K. M., Adkins, J. F., Sodemann, H., Clark, B., and Tuen, A. A.: Diurnal to interannual rainfall \$\delta^{18}\text{O}\$ variations in northern Borneo driven by regional hydrology, *Earth and Planetary Science Letters*, 369–370, 108–119, <https://doi.org/10.1016/j.epsl.2013.03.014>, 2013.](#)
- 1205 [Muller, C. L., Baker, A., Fairchild, I. J., Kidd, C., and Boomer, I.: Intra-Event Trends in Stable Isotopes: Exploring Midlatitude Precipitation Using a Vertically Pointing Micro Rain Radar, *Journal of Hydrometeorology*, 16, 194–213, <https://doi.org/10.1175/JHM-D-14-0038.1>, 2015.](#)
- 1210 [Munksgaard, N. C., Kurita, N., Sánchez-Murillo, R., Ahmed, N., Araguas, L., Balachew, D. L., Bird, M. I., Chakraborty, S., Kien Chinh, N., Cobb, K. M., Ellis, S. A., Esquivel-Hernández, G., Ganyaglo, S. Y., Gao, J., Gastmans, D., Kaseke, K. F., Kebede, S., Morales, M. R., Mueller, M., Poh, S. C., Santos, V. dos, Shaoneng, H., Wang, L., Yacobaccio, H., and Zwart, C.: Data Descriptor: Daily observations of stable isotope ratios of rainfall in the tropics, *Scientific Reports*, 9, 1–7, <https://doi.org/10.1038/s41598-019-50973-9>, 2019.](#)
- 1215 [R Core Team: A language and environment for statistical computing, R Foundation for Statistical Computing, Vienna, Austria, <https://www.R-project.org/>, 2023.](#)
- [Rao, N. T., Kirankumar, N. V. P., Radhakrishna, B., and Rao, N. D.: Classification of tropical precipitating systems using wind profiler spectral moments. Part I: Algorithm description and validation, *Journal of Atmospheric and Oceanic Technology*, 25, 884–897, <https://doi.org/10.1175/2007JTECHA1031.1>, 2008.](#)
- 1220 [Ribeiro, B. Z., Machado, L. A. T., Biscaro, T. S., Freitas, E. D., Mozer, K. W., and Goodman, S. J.: An evaluation of the GOES-16 rapid scan for nowcasting in southeastern Brazil: Analysis of a severe hailstorm case, *Weather and Forecasting*, 34, 1829–1848, <https://doi.org/10.1175/WAF-D-19-0070.1>, 2019.](#)
- [Risi, C., Bony, S., and Vimeux, F.: Influence of convective processes on the isotopic composition \(\$\delta^{18}\text{O}\$ and \$\delta\text{D}\$ \) of precipitation and water vapor in the tropics: 2. Physical interpretation of the amount effect, *Journal of Geophysical Research Atmospheres*, 113, 1–12, <https://doi.org/10.1029/2008JD009943>, 2008.](#)
- 1225 [Risi, C., Bony, S., Vimeux, F., Chongd, M., and Descroix, L.: Evolution of the stable water isotopic composition of the rain sampled along Sahelian squall lines, *Quarterly Journal of the Royal Meteorological Society*, 136, 227–242, <https://doi.org/10.1002/qj.485>, 2010.](#)

1230 [Risi, C., Galewsky, J., Reverdin, G., and Brient, F.: Controls on the water vapor isotopic composition near the surface of tropical oceans and role of boundary layer mixing processes, *Atmospheric Chemistry and Physics*, 19, 12235–12260, <https://doi.org/10.5194/acp-19-12235-2019>, 2019.](#)

[Roberts, R. D. and Rutledge, S.: Nowcasting storm initiation and growth using GOES-8 and WSR-88D data, *Weather and Forecasting*, 18, 562–584, \[https://doi.org/10.1175/1520-0434\\(2003\\)018<0562:NSIAGU>2.0.CO;2\]\(https://doi.org/10.1175/1520-0434\(2003\)018<0562:NSIAGU>2.0.CO;2\), 2003.](#)

[Roca, R. and Fiolleau, T.: Extreme precipitation in the tropics is closely associated with long-lived convective systems, *Communications Earth & Environment*, 1, 18, <https://doi.org/10.1038/s43247-020-00015-4>, 2020.](#)

1235 [Romatschke, U. and Houze, R. A.: Characteristics of precipitating convective systems accounting for the summer rainfall of tropical and subtropical South America, *Journal of Hydrometeorology*, 14, 25–46, <https://doi.org/10.1175/JHM-D-12-060.1>, 2013.](#)

[Rozanski, K., Sonntag, C., and Munnich, K. O.: Factors controlling stable isotope composition of European precipitation., *Tellus*, 34, 142–150, <https://doi.org/10.3402/tellusa.v34i2.10796>, 1982.](#)

1240 [Rozanski, K., Araguás-Araguás, L., and Gonfiantini, R.: Isotopic Patterns in Modern Global Precipitation, 1–36, <https://doi.org/10.1029/GM078p0001>, 1993.](#)

[Salati, E., Dall'Olio, A., Matsui, E., and Gat, J. R.: Recycling of water in the Amazon Basin: An isotopic study, *Water Resources Research*, 15, 1250–1258, <https://doi.org/10.1029/WR015i005p01250>, 1979.](#)

1245 [Sánchez-Murillo, R., Durán-Quesada, A. M., Birkel, C., Esquivel-Hernández, G., and Boll, J.: Tropical precipitation anomalies and d-excess evolution during El Niño 2014–16, *Hydrological Processes*, 31, 956–967, <https://doi.org/10.1002/hyp.11088>, 2017.](#)

[Sánchez-Murillo, R., Durán-Quesada, A. M., Esquivel-Hernández, G., Rojas-Cantillano, D., Birkel, C., Welsh, K., Sánchez-Llull, M., Alonso-Hernández, C. M., Tetzlaff, D., Soulsby, C., Boll, J., Kurita, N., and Cobb, K. M.: Deciphering key processes](#)

1250 [controlling rainfall isotopic variability during extreme tropical cyclones, *Nature Communications*, 10, 1–10, <https://doi.org/10.1038/s41467-019-12062-3>, 2019.](#)

[dos Santos, V., Gastmans, D., and Sánchez-Murillo, R.: Isotope and meteorologic database of high-frequency sampling of convective rainfall events in Rio Claro, Brazil, <https://doi.org/10.17632/kk3gs8zn4s.1>, 2023.](#)

[Sarkar, M., Bailey, A., Blossy, P., de Szoeko, S. P., Noone, D., Quiñones Meléndez, E., Leandro, M. D., and Chuang, P. Y.:](#)

1255 [Sub-cloud rain evaporation in the North Atlantic winter trade winds derived by pairing isotopic data with a bin-resolved microphysical model, *Atmospheric Chemistry and Physics*, 23, 12671–12690, <https://doi.org/10.5194/acp-23-12671-2023>, 2023.](#)

[Schmit, T. J., Griffith, P., Gunshor, M. M., Daniels, J. M., Goodman, S. J., and Lebair, W. J.: A closer look at the ABI on the goes-r series, *Bulletin of the American Meteorological Society*, 98, 681–698, <https://doi.org/10.1175/BAMS-D-15-00230.1>,](#)

1260 [2017.](#)

[Shapiro, S. S.; Wilk, M. B.: An analysis of variance test for normality \(complete samples\), *Biometrika*, 53, 591–611, 1965.](#)

[Siqueira, J. R. and Machado, L. A. T.: Influence of the frontal systems on the day-to-day convection variability over South](#)

America, *Journal of Climate*, 17, 1754–1766, [https://doi.org/10.1175/1520-0442\(2004\)017<1754:IOTFSO>2.0.CO;2](https://doi.org/10.1175/1520-0442(2004)017<1754:IOTFSO>2.0.CO;2), 2004.

Siqueira, J. R., Rossow, W. B., Machado, L. A. T., and Pearl, C.: Structural characteristics of convective systems over South America related to cold-frontal incursions, *Monthly Weather Review*, 133, 1045–1064, <https://doi.org/10.1175/MWR2888.1.2005>.

Soderberg, K., Good, S. P., O’connor, M., Wang, L., Ryan, K., and Caylor, K. K.: Using atmospheric trajectories to model the isotopic composition of rainfall in central Kenya, *Ecosphere*, 4, 1–18, <https://doi.org/10.1890/ES12-00160.1>, 2013.

Stein, A. F., Draxler, R. R., Rolph, G. D., Stunder, B. J. B., Cohen, M. D., and Ngan, F.: NOAA’s hysplit atmospheric transport and dispersion modeling system, *Bulletin of the American Meteorological Society*, 96, 2059–2077, <https://doi.org/10.1175/BAMS-D-14-00110.1>, 2015.

Steiner, M. and Smith, J. A.: Convective versus stratiform rainfall: An ice-microphysical and kinematic conceptual model, *Atmospheric Research*, 47–48, 317–326, [https://doi.org/10.1016/S0169-8095\(97\)00086-0](https://doi.org/10.1016/S0169-8095(97)00086-0), 1998.

Stewart, M. K.: Stable isotope fractionation due to evaporation and isotopic exchange of falling waterdrops: Applications to atmospheric processes and evaporation of lakes, *Journal of Geophysical Research*, 80, 1133–1146, <https://doi.org/10.1029/JC080i009p01133>, 1975.

Sun, C., Shanahan, T. M., and Partin, J.: Controls on the isotopic composition of precipitation in the South-Central United States, *Journal of Geophysical Research: Atmospheres*, 124, 8320–8335, <https://doi.org/10.1029/2018JD029306>, 2019.

Sun, C., Tian, L., Shanahan, T. M., Partin, J. W., Gao, Y., Piatrunia, N., and Banner, J.: Isotopic variability in tropical cyclone precipitation is controlled by Rayleigh distillation and cloud microphysics, *Communications Earth & Environment*, 3, <https://doi.org/10.1038/s43247-022-00381-1>, 2022.

Taupin, J.-D., Gallaire, R., and Arnaud, Y.: Analyses isotopiques et chimiques des précipitations sahélienne de la région de Niamey au Niger: implications climatologiques, *Hydrochemistry*, 151–162, 1997.

Torri, G.: On the isotopic composition of cold pools in radiative-convective equilibrium, *Journal of Geophysical Research: Atmospheres*, 126, 1–20, <https://doi.org/10.1029/2020JD033139>, 2021.

Tremoy, G., Vimeux, F., Soumana, S., Souley, I., Risi, C., Favreau, G., and Oï, M.: Clustering mesoscale convective systems with laser-based water vapor $\delta^{18}\text{O}$ monitoring in Niamey (Niger), *Journal of Geophysical Research: Atmospheres*, 119, 5079–5103, <https://doi.org/10.1002/2013JD020968>, 2014.

Vila, D. A., Machado, L. A. T., Laurent, H., and Velasco, I.: Forecast and tracking the evolution of cloud clusters (ForTraCC) using satellite infrared imagery: Methodology and validation, *Weather and Forecasting*, 23, 233–245, <https://doi.org/10.1175/2007WAF2006121.1>, 2008.

de Vries, A. J., Aemisegger, F., Pfahl, S., and Wernli, H.: Stable water isotope signals in tropical ice clouds in the West African monsoon simulated with a regional convection-permitting model, *Atmospheric Chemistry and Physics*, 22, 8863–8895, <https://doi.org/10.5194/acp-22-8863-2022>, 2022.

World Meteorological Organization: WMO Atlas of Mortality and Economic Losses From Weather , Climate and Water Extremes (1970-2019), Geneva 2, Switzerland, 90 pp., 2021.

Zawadzki, I. and Antonio, M. D. A.: Equilibrium Raindrop Size Distributions in Tropical Rain, *Journal of the Atmospheric Sciences*, 45, 3452–3459, [https://doi.org/10.1175/1520-0469\(1988\)045<3452:ERSDIT>2.0.CO;2](https://doi.org/10.1175/1520-0469(1988)045<3452:ERSDIT>2.0.CO;2), 1988.

Zilli, M. T., Carvalho, L. M. V., Liebmann, B., and Silva Dias, M. A.: A comprehensive analysis of trends in extreme precipitation over southeastern coast of Brazil, *International Journal of Climatology*, 37, 2269–2279, <https://doi.org/10.1002/joc.4840>, 2017.

Zwart, C., Munksgaard, N. C., Protat, A., Kurita, N., Lambrinidis, D., and Bird, M. I.: The isotopic signature of monsoon conditions, cloud modes, and rainfall type, *Hydrological Processes*, 32, 2296–2303, <https://doi.org/10.1002/hyp.13140>, 2018.

Table 1. Summarizing overall convective rainfall events and median values of isotope and meteorological parameters.

Season	Daytime	Data	Number of samples	Duration	Isotopes			Automatic Weather Station					Micro-Rain Radar		GOES- 16
					$\delta^{18}\text{O}$	$\delta^2\text{H}$	d -excess	Rain-rate	RH	T	Tdw	LCL	Z	w	BT
-	-	-	n	minutes	‰			mm.min ⁻¹	%	°C	meters	dBZ	m.s ⁻¹	°C	
Spring	Day	05/11/2019	21	82	-3.1	0.8	22.9	0.4	96	21	20	146	46	8.0	-63
Spring	Day	18/11/2020	8	141	-4.2	-13.7	19.7	0.2	86	20	17	489	38	7.1	-63
Autumn	Day	09/06/2020	12	96	-3.4	-5.6	17.3	0.3	95	19	18	168	42	7.7	-50
Autumn	Night	23/05/2020	4	131	-2.9	-6.9	16.3	0.0	87	19	17	449	33	6.6	-56
Summer	Night	30/01/2020	6	23	-10.0	-64.4	15.7	0.4	93	23	21	247	38	6.6	-53
Summer	Night	10/02/2020	18	86	-13.9	-92.0	17.5	0.5	97	22	21	93	41	6.7	-39
Summer	Day	01/02/2020	5	18	-10.4	-73.5	13.4	0.6	93	23	21	253	39	7.1	-60
Summer	Day	24/02/2021	16	55	-6.8	-44.8	7.2	0.5	86	21	18	468	35	7.1	-51

1310 -RH = Relative Humidity, T = Temperature, Tdw = Dew point temperature, LCL = Lifting condensation level, Z = Reflectivity, w = fall velocity and Brightness temperature.

Table 1. Summarizing overall convective rainfall events, isotope and meteorological parameters

<u>Season</u>		<u>Spring</u>		<u>Autumn</u>		<u>Summer</u>			
<u>Data</u>		<u>2019/11/05</u>	<u>2020/11/18</u>	<u>2020/05/23</u>	<u>2020/06/09</u>	<u>2020/01/30</u>	<u>2020/02/10</u>	<u>2020/02/01</u>	<u>2021/02/24</u>
<u>Number of samples</u>		<u>21</u>	<u>8</u>	<u>4</u>	<u>12</u>	<u>6</u>	<u>18</u>	<u>5</u>	<u>16</u>
<u>Duration</u>		<u>82</u>	<u>141</u>	<u>131</u>	<u>96</u>	<u>23</u>	<u>86</u>	<u>18</u>	<u>55</u>
<u>δ¹⁸O</u>	<u>Initial</u>	<u>-3.0</u>	<u>-2.7</u>	<u>-2.6</u>	<u>-3.6</u>	<u>-10.1</u>	<u>-12.3</u>	<u>-10.2</u>	<u>-7.6</u>
	<u>Median</u>	<u>-3.1</u>	<u>-4.2</u>	<u>-2.9</u>	<u>-3.4</u>	<u>-10</u>	<u>-13.9</u>	<u>-10.4</u>	<u>-6.8</u>
	<u>Δδ</u>	<u>2.4</u>	<u>2.6</u>	<u>0.8</u>	<u>2.2</u>	<u>1.1</u>	<u>7.3</u>	<u>1.5</u>	<u>3.5</u>
<u>δ²H</u>	<u>Initial</u>	<u>3.4</u>	<u>-4.6</u>	<u>-4.6</u>	<u>-5.2</u>	<u>-60.1</u>	<u>-86.6</u>	<u>-71.0</u>	<u>-47.8</u>
	<u>Median</u>	<u>0.8</u>	<u>-13.7</u>	<u>-6.9</u>	<u>-5.6</u>	<u>-64.4</u>	<u>-92.0</u>	<u>-73.5</u>	<u>-44.8</u>
	<u>Δδ</u>	<u>16.9</u>	<u>9.9</u>	<u>8.9</u>	<u>11</u>	<u>10.5</u>	<u>43.1</u>	<u>7.4</u>	<u>20.9</u>
<u>d-excess</u>	<u>Initial</u>	<u>27.4</u>	<u>10.2</u>	<u>16.7</u>	<u>24.1</u>	<u>20.8</u>	<u>12.1</u>	<u>11.3</u>	<u>13.0</u>
	<u>Median</u>	<u>22.9</u>	<u>19.7</u>	<u>16.3</u>	<u>17.3</u>	<u>15.7</u>	<u>17.5</u>	<u>13.4</u>	<u>7.2</u>
	<u>Δδ</u>	<u>7.1</u>	<u>12.8</u>	<u>4.0</u>	<u>19.2</u>	<u>9.5</u>	<u>16.6</u>	<u>8.4</u>	<u>17.2</u>
<u>Automatic Weather Station</u>	<u>Rain rate</u>	<u>0.4</u>	<u>0.2</u>	<u>0.1</u>	<u>0.3</u>	<u>0.4</u>	<u>0.5</u>	<u>0.6</u>	<u>0.5</u>
	<u>RH</u>	<u>96</u>	<u>85</u>	<u>87</u>	<u>95</u>	<u>93</u>	<u>97</u>	<u>93</u>	<u>86</u>
	<u>T</u>	<u>21</u>	<u>20</u>	<u>19</u>	<u>19</u>	<u>23</u>	<u>22</u>	<u>23</u>	<u>21</u>
	<u>Tdw</u>	<u>20</u>	<u>17</u>	<u>17</u>	<u>18</u>	<u>21</u>	<u>21</u>	<u>21</u>	<u>18</u>
	<u>LCL</u>	<u>146</u>	<u>489</u>	<u>449</u>	<u>168</u>	<u>247</u>	<u>93</u>	<u>253</u>	<u>468</u>
<u>Micro Rain Radar</u>	<u>Zc</u>	<u>46</u>	<u>38</u>	<u>33</u>	<u>42</u>	<u>38</u>	<u>41</u>	<u>39</u>	<u>35</u>
	<u>w</u>	<u>8</u>	<u>7.1</u>	<u>6.6</u>	<u>7.7</u>	<u>6.6</u>	<u>6.7</u>	<u>7.1</u>	<u>7.1</u>
<u>GOES-16</u>	<u>BT</u>	<u>-63</u>	<u>-63</u>	<u>-56</u>	<u>-50</u>	<u>-53</u>	<u>-39</u>	<u>-60</u>	<u>-51</u>

Duration (minutes); Isotopes parameters (‰); Median values of meteorological variables: Rain rate (mm.min⁻¹), Relative Humidity – (RH %), Temperature (T °C), Dew Temperature (Tdw °C), Lifting Condensation Level (LCL meters), Reflectivity (Zc dBZ), Vertical Velocity (m.s⁻¹) and Brightness temperature (BT °C).

Table 2. The results of semi-quantitative assessment of the impact of below-cloud processes on the isotope characteristics of convective precipitation

Rainfall event	T_{INT.}^{a)} (°C)	RH_{INT.}^{b)} (%)	F^{c)} (-)	Δd-excess^{d)} (‰)
<u>The 10/02/2020 event</u> δ _v — isotopic composition of rainfall (‰): δ ² H = -91.97, δ ¹⁸ O = -13.85, d-excess = 18.8 δ _A — isotopic composition of equilibrium vapour (‰) ^{e)} : δ ² H = -161.6, δ ¹⁸ O = -23.28, d-excess = 24.6	21.7	98.6	0.9994	0.1
<u>The 24/02/2021 day-time event</u> δ _v — isotopic composition of rainfall (‰): δ ² H = -44.8, δ ¹⁸ O = -6.79, d-excess = 9.5 δ _A — isotopic composition of equilibrium vapour (‰): δ ² H = -120.3, δ ¹⁸ O = -16.48, d-excess = 11.5	19.3	93.2	0.9800	3.0

a) mean temperature of below cloud ambient atmosphere (linear interpolation between cloud-base and ground-level values)

b) mean relative humidity of below cloud ambient atmosphere (linear interpolation between cloud-base and ground-level values)

c) remaining mass fraction of raindrops after their travel from the cloud-base to the surface (see text)

d) reduction of the d-excess of raindrops as a result of their travel from the cloud-base to the surface (see text)

e) assumed isotopic composition of ambient humid atmosphere below the cloud-base derived from the measured isotopic composition of rainfall and ground-level temperature.

Table 2. The results of semi-quantitative assessment of the impact of below-cloud processes on the isotope characteristics of convective precipitation

Rainfall event	T_{INT.}^{a)} (°C)	RH_{INT.}^{b)} (%)	F^{c)} (-)	Δd-excess^{d)} (‰)
<u>The 2019/11/05 event</u> δ _v - isotopic composition of rainfall (‰): δ ² H = 0.80, δ ¹⁸ O = -3.11, d-excess = 25.7 δ _A - isotopic composition of equilibrium vapour (‰) ^{e)} : δ ² H = -78.3, δ ¹⁸ O = -12.84, d-excess = 24.4	19.3	97.8	0.9982	1.7
<u>The 2020/11/18</u> δ _v - isotopic composition of rainfall (‰): δ ² H = -13.7, δ ¹⁸ O = -4.16, d-excess = 19.5 δ _A - isotopic composition of equilibrium vapour (‰): δ ² H = -93.2, δ ¹⁸ O = -14.01, d-excess = 18.8	19.0	92.9	0.9795	3.1
<u>The 2020/05/23</u> δ _v - isotopic composition of rainfall (‰): δ ² H = -6.9, δ ¹⁸ O = -2.89, d-excess = 16.2 δ _A - isotopic composition of equilibrium vapour (‰): δ ² H = -86.6, δ ¹⁸ O = -12.72, d-excess = 15.2	18.1	93.4	0.9806	2.8

Formatado: Inglês (Estados Unidos)

<u>The 2020/06/09</u>	<u>19.3</u>	<u>97.5</u>	<u>0.9978</u>	<u>0.2</u>
<u>δ_o - isotopic composition of rainfall (‰):</u>				
<u>$\delta^2\text{H} = -5.5$, $\delta^{18}\text{O} = -3.37$, $d\text{-excess} = 21.3$</u>				
<u>δ_A - isotopic composition of equilibrium vapour (‰):</u>				
<u>$\delta^2\text{H} = -84.8$ $\delta^{18}\text{O} = -13.15$, $d\text{-excess} = 20.4$</u>				
<u>The 2020/01/30</u>	<u>22.4</u>	<u>96.4</u>	<u>0.9944</u>	<u>0.9</u>
<u>δ_o - isotopic composition of rainfall (‰):</u>				
<u>$\delta^2\text{H} = -64.4$, $\delta^{18}\text{O} = -10.03$, $d\text{-excess} = 15.8$</u>				
<u>δ_A - isotopic composition of equilibrium vapour (‰):</u>				
<u>$\delta^2\text{H} = -135.5$ $\delta^{18}\text{O} = -19.44$, $d\text{-excess} = 20.0$</u>				
<u>The 2020/02/10</u>	<u>21.7</u>	<u>98.6</u>	<u>0.9994</u>	<u>0.1</u>
<u>δ_o - isotopic composition of rainfall (‰):</u>				
<u>$\delta^2\text{H} = -91.97$, $\delta^{18}\text{O} = -13.85$, $d\text{-excess} = 18.8$</u>				
<u>δ_A - isotopic composition of equilibrium vapour (‰):</u>				
<u>$\delta^2\text{H} = -161.6$ $\delta^{18}\text{O} = -23.28$, $d\text{-excess} = 24.6$</u>				
<u>The 2020/02/01</u>	<u>22.5</u>	<u>96.3</u>	<u>0.9947</u>	<u>0.9</u>
<u>δ_o - isotopic composition of rainfall (‰):</u>				
<u>$\delta^2\text{H} = -73.5$, $\delta^{18}\text{O} = -10.44$, $d\text{-excess} = 10.2$</u>				
<u>δ_A - isotopic composition of equilibrium vapour (‰):</u>				
<u>$\delta^2\text{H} = -143.8$ $\delta^{18}\text{O} = -19.80$, $d\text{-excess} = 14.6$</u>				
<u>The 2021/02/24</u>	<u>19.3</u>	<u>93.2</u>	<u>0.9800</u>	<u>3.0</u>
<u>δ_o - isotopic composition of rainfall (‰):</u>				
<u>$\delta^2\text{H} = -44.8$, $\delta^{18}\text{O} = -6.79$, $d\text{-excess} = 9.5$</u>				
<u>δ_A - isotopic composition of equilibrium vapour (‰):</u>				
<u>$\delta^2\text{H} = -120.3$ $\delta^{18}\text{O} = -16.48$, $d\text{-excess} = 11.5$</u>				

a) mean temperature of below cloud ambient atmosphere (linear interpolation between cloud base and ground level values)

b) mean relative humidity of below cloud ambient atmosphere (linear interpolation between cloud base and ground level values)

c) remaining mass fraction of raindrops after their travel from the cloud base to the surface (see text)

d) reduction of the $d\text{-excess}$ of raindrops as a result of their travel from the cloud base to the surface (see text)

e) assumed isotopic composition of ambient humid atmosphere below the cloud base derived from the measured isotopic composition of rainfall and ground-level temperature.

1330

1335

1340

1345

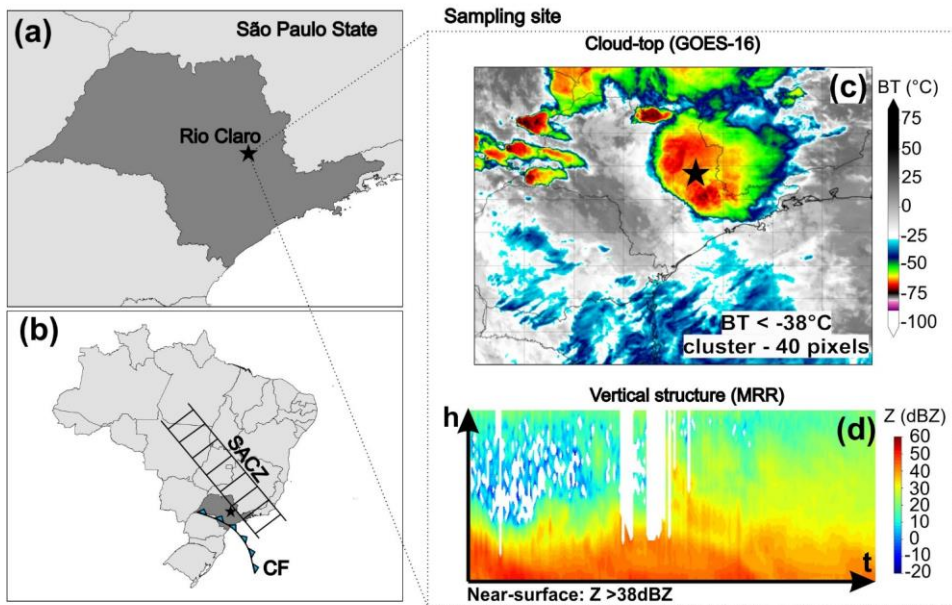


Figure 1. (a) Localization of sampling site in Rio Claro (black star) (b) in regional-synoptic context across Brazil and main weather systems (CF – cold front and SACZ – Southern Atlantic Convergence Zone). Over-collection point (c) GOES-16 satellite imagery showed convective system with lower brightness temperature (BT, cloud-top) and (d) Micro Rain Radar (MRR) illustrates the vertical structure of convective rainfall, height (h) and time (t), characterized by radar reflectivity (Z) with strong values near-surface. Regional and local context of study area. (a) Localization of sampling site in Rio Claro (black star) (b) regional synoptic context across Brazil and main weather systems (CF – cold front and SACZ – Southern Atlantic Convergence Zone). (c) GOES-16 satellite imagery of convective rainfall (d) Micro Rain Radar (MRR) image of convective rainfall.

1350

1355

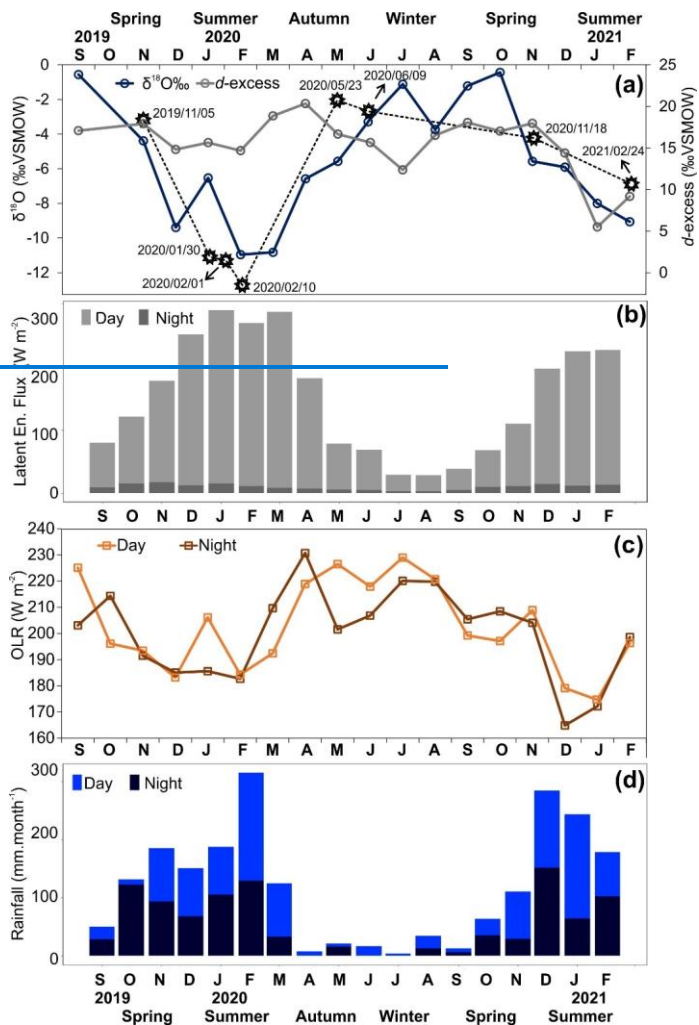


Figure 2. (a) Seasonal variation of $\delta^{18}\text{O}$ and d -excess values in monthly rainfall and aggregated monthly $\delta^{18}\text{O}$ values high-frequency convective rainfall sampling discussed in this study (b) AQUA/AIRS latent heat flux. (c) MERRA-2 outgoing longwave radiation (monthly averaged daytime and night-time data) (d) monthly-rainfall amounts at Rio Claro separated into day and night fraction (no rainfall types distinguished). The star symbol indicates the collected high-frequency events, ranked according to average values of $\delta^{18}\text{O}$.

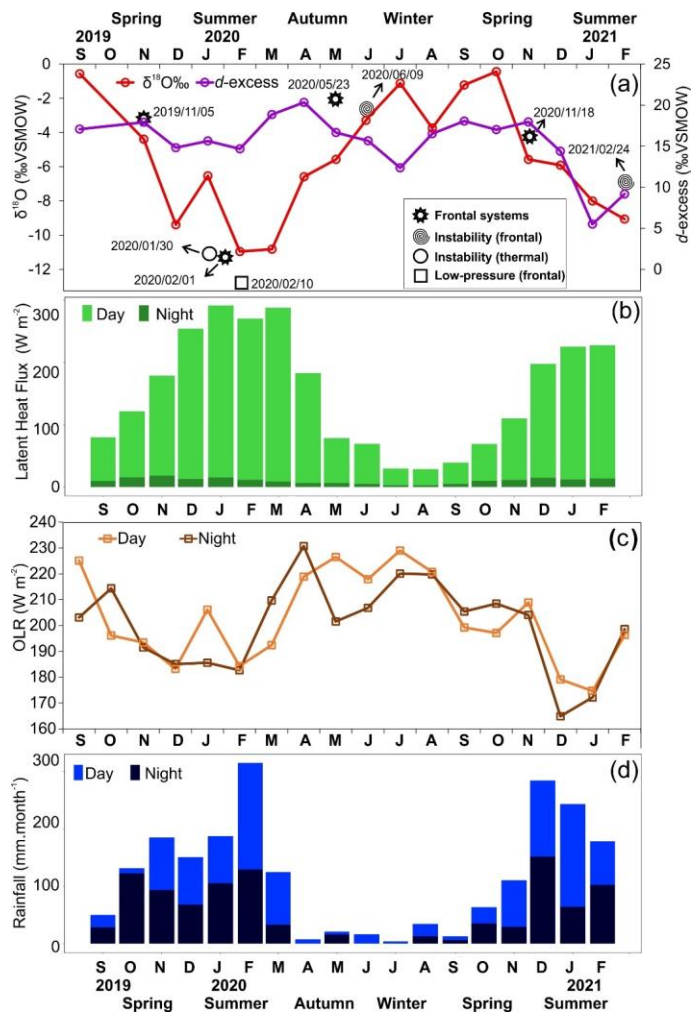
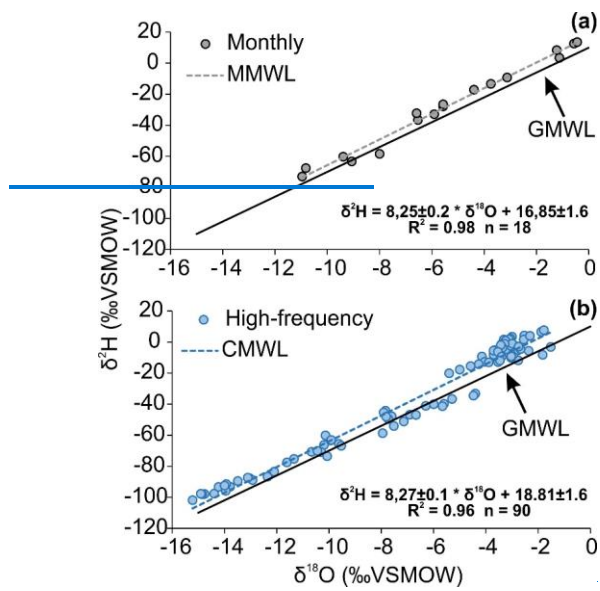


Figure 2. Seasonal variation of isotope and convective parameters. (a) Temporal distribution of monthly $\delta^{18}\text{O}$ and d -excess values during study period, with aggregated median of $\delta^{18}\text{O}$ values for high-frequency convective rainfall events (b) AQUA/AIRS latent heat flux. (c) MERRA-2 outgoing longwave radiation (monthly averaged daytime and night-time data) (d) monthly rainfall amounts at Rio Claro separated into day and night fraction (no rainfall types distinguished). The black symbol indicates weather systems described in section 3.1. The monthly isotopic composition used in this figure was collected by the first authors of the article and determined by the UNESP laboratory, following the same procedures mentioned in section 2.2.



375 **Figure 3.** (a) Monthly and (b) high-frequency $\delta^{2}\text{H}$ and $\delta^{18}\text{O}$ rainfall data plotted in the $\delta^{2}\text{H}/\delta^{18}\text{O}$ space. LMWL—local meteoric water line based on monthly values, CMWL—convective meteoric water line and GMWL—global meteoric water line.

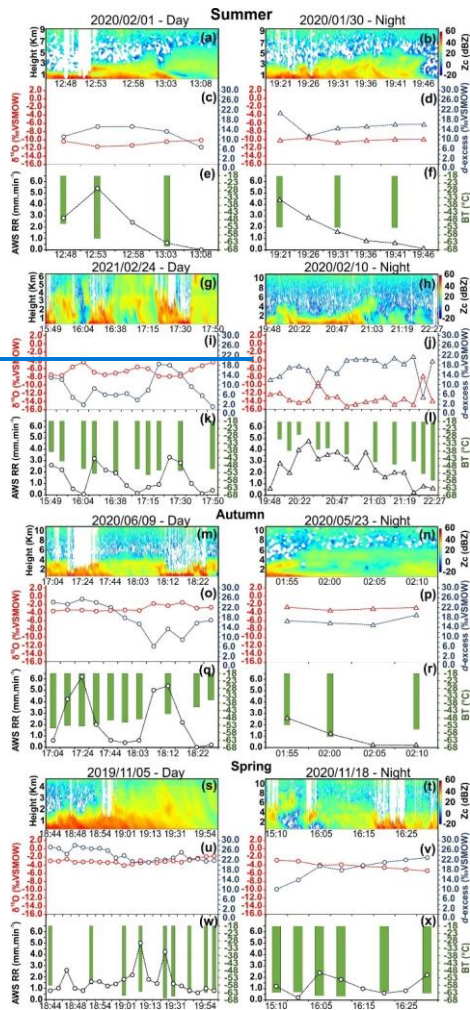


Figure 4. Intra-event variability of eight convective rainfall sampling. For summer season, 2020/02/01 (a, c, e), 2020/01/30 (b, d, f), 24/02/21 (g, i, k) and 2020/02/10 (h, j, l), autumn, 09/06/2020 (m, o, q) and 23/05/2020 (n, p, r), autumn 05/11/2019 (s, u, w) and 18/11/2020 (t, v, x). $\delta^{18}\text{O}$ is red color, d excess is orange, rain rate (RR) in dark blue, brightness temperature (BT) in green. The Z_c is the corrected reflectivity of Micro Rain Radar plotted as vertical profile.

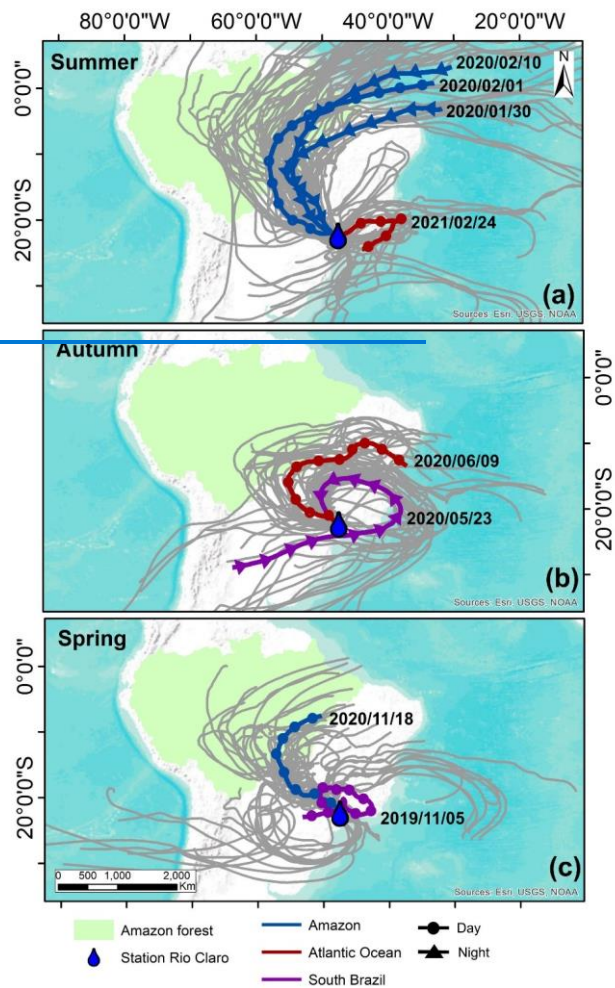


Figure 5. Ten-day backward trajectories arriving at Rio Claro station of eight convective events on (a) Summer, (b) Autumn and (c) Spring. Twenty-seven ensembles are grey lines, and the mean trajectory is the colors lines. The colours of the mean trajectories indicate the origin of air masses: blue influenced by Amazon Forest, Tuscan red from Atlantic Ocean and Purple from South Brazil portion. Symbols are daytime of convective events, day (circle) and night (triangle). The authors used trivial information, the borders of the countries and the ocean provided by the ESRI base map.

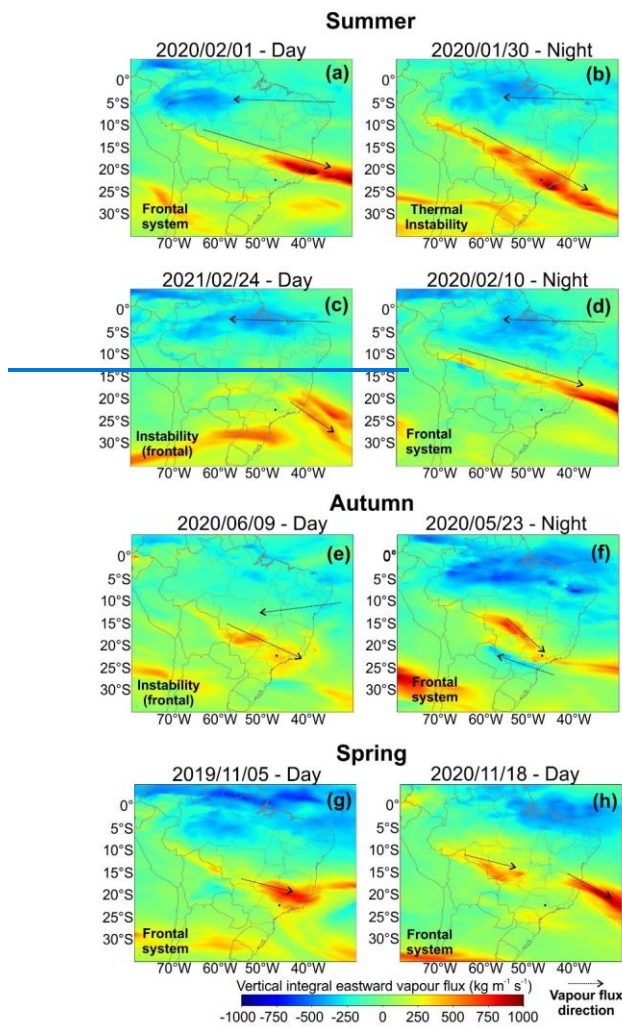


Figure 6. ERA-5 vertical integral of eastward water vapor flux for the days when convective rainfall events occurred, during (a, b, c, d) summer, (e, f) autumn and (g, h) spring aggregated with weather systems text. Positive values indicate the direction of moisture vapor flux from left to right, and negative values from right to left. Arrows illustrate the direction of vapour flux. The weather systems are indicated for each rainfall event.

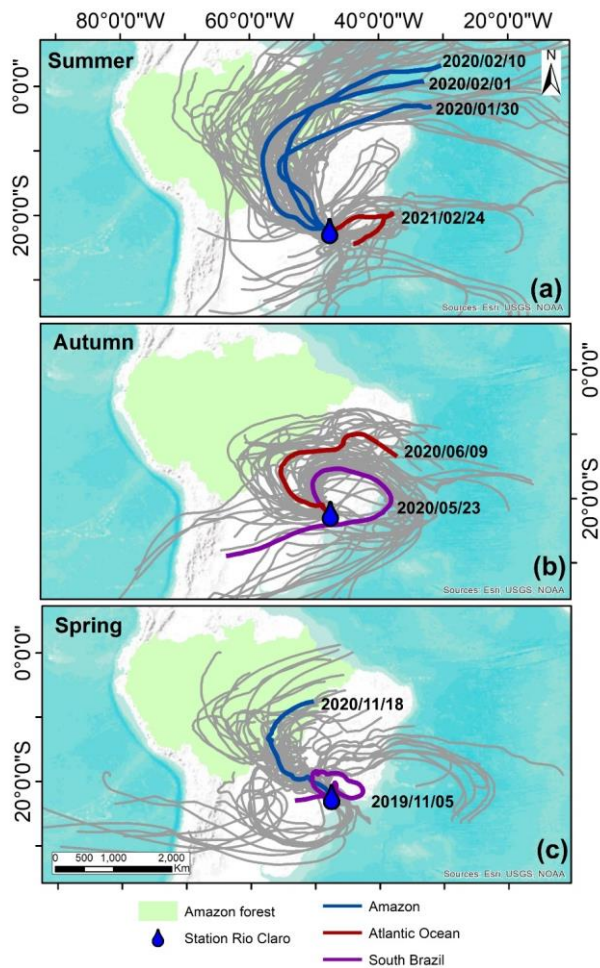


Figure 3. Ten-day backward trajectories arriving at Rio Claro station of eight convective events. (a) Summer, (b) Autumn and (c) Spring. Twenty-seven ensembles are grey lines, and the mean trajectory is the colors lines. The colours of the mean trajectories indicate the origin of air masses. The authors used trivial information, the borders of the countries and the ocean provided by the ESRI base map.

1395

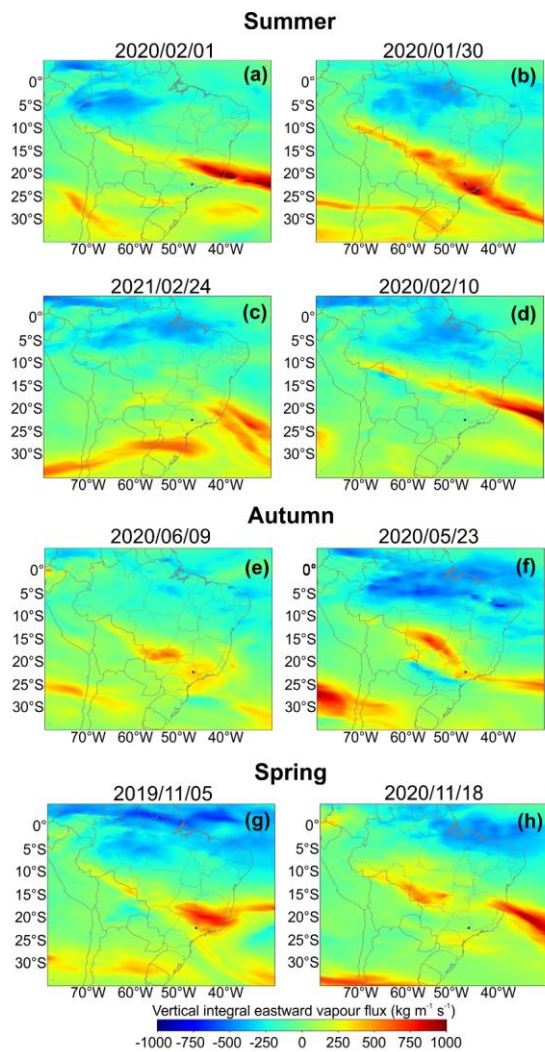


Figure 4. ERA-5 vertical integral of eastward water vapor flux. (a, b, c, d) summer convective events (e, f) autumn and (g, h) spring aggregated. The maps corresponded to the days when convective rainfall events occurred. Positive values indicate the direction of moisture vapor flux from left to right, and negative values from right to left.

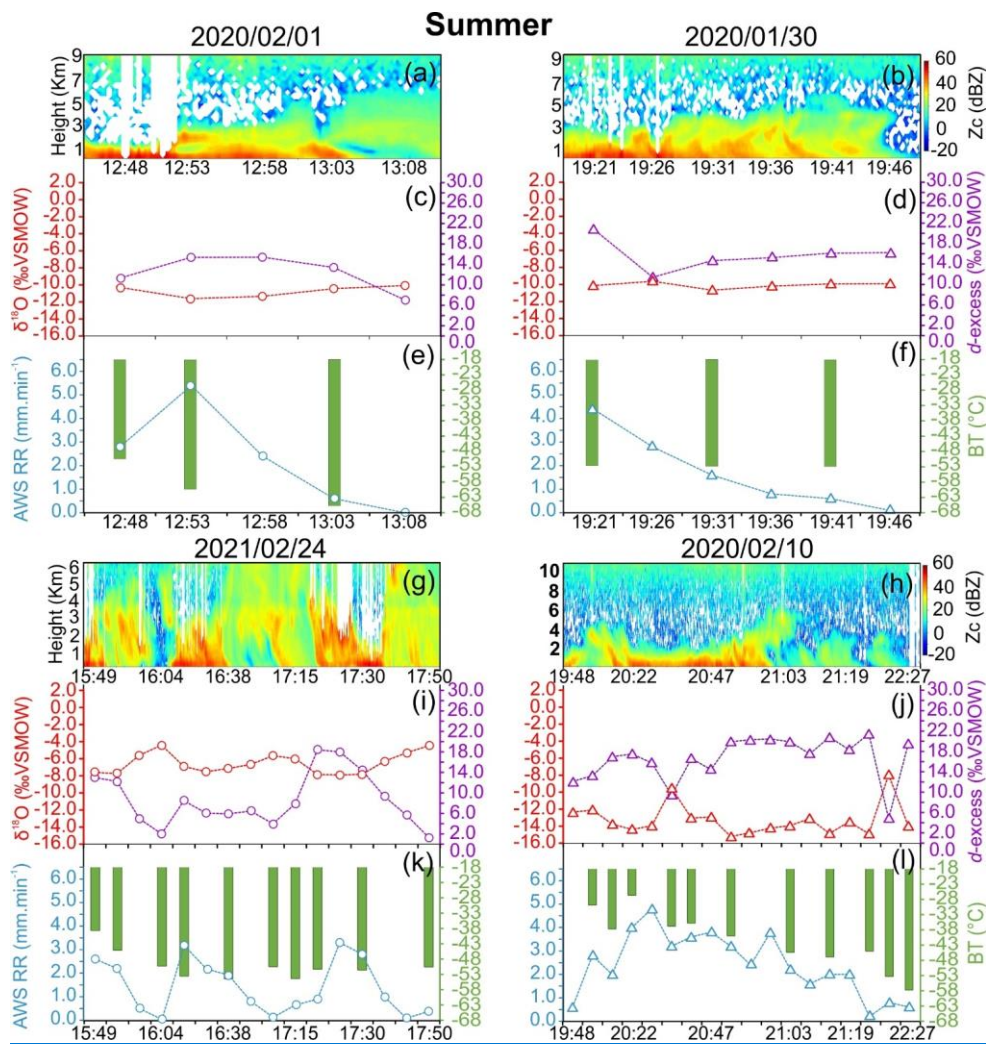


Figure 5. Summer intra-events. (a, b, g, h) radar reflectivity of Micro Rain Radar (c, d, i, j) $\delta^{18}O$ (red lines) and d -excess (purple lines) (e, f, k, l) brightness temperature (BT – green bars) and rainfall amount (blue lines).

1405

Formatado: Normal, À esquerda

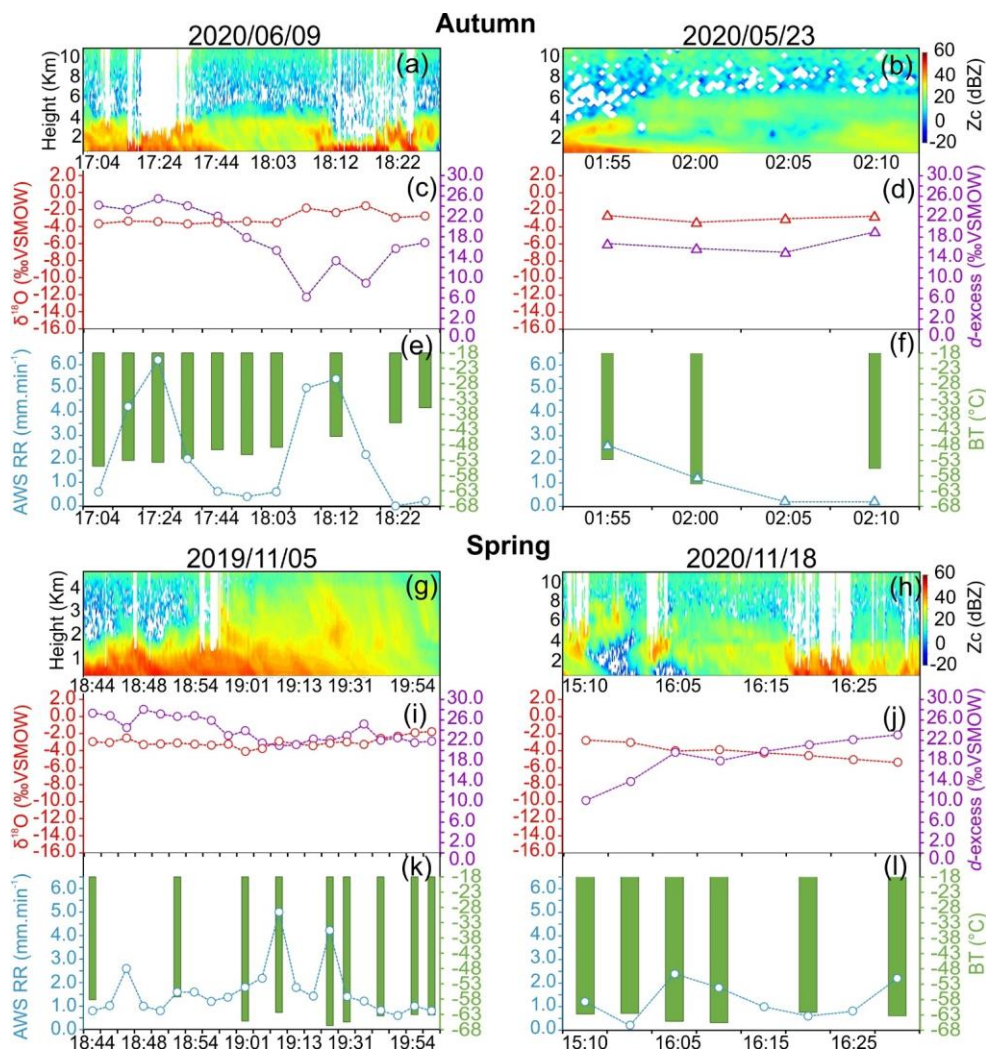


Figure 6. Autumn and spring intra-events. Refer to Fig. 5 for legend description.

Formatado: Normal, À esquerda